

# Redox-Active Tetraruthenium Macrocycles Built from 1,4-Divinylphenylene-Bridged Diruthenium Complexes

Stefan Scheerer,<sup>[a]</sup> Michael Linseis,<sup>[a]</sup> Evelyn Wuttke,<sup>[a, d]</sup> Sabrina Weickert,<sup>[a]</sup> Malte Drescher,<sup>[a]</sup> Oliver Tröppner,<sup>[b]</sup> Ivana Ivanović-Burmazović,<sup>[b]</sup> Andreas Irmeler,<sup>[c]</sup> Fabian Pauly,<sup>\*[c]</sup> and Rainer F. Winter<sup>\*[a]</sup>

**Abstract:** Metallamacrocyclic tetraruthenium complexes were generated by treatment of 1,4-divinylphenylene-bridged diruthenium complexes with functionalized 1,3-benzene dicarboxylic acids and characterized by HR ESI-MS and multinuclear NMR spectroscopy. Every divinylphenylene diruthenium subunit is oxidized in two consecutive one-electron steps with half-wave potential splittings in the range of 250 to 330 mV. Additional, smaller redox-splittings between the +/2+ and 0/+ and the 3+/4+ and 2+/3+ redox processes, corresponding to the first and the second oxidations of every divinylphenylene diruthenium entity, are due to electrostatic effects. The lack of electronic coupling through bond or through space is explained by the nodal properties

of the relevant molecular orbitals and the lateral side-by-side arrangement of the divinylphenylene linkers. The polyelectrochromic behavior of the divinylphenylene diruthenium precursors is retained and even amplified in these metallamacrocyclic structures. EPR studies down to  $T=4$  K indicate that the dications **1-H**<sup>2+</sup> and **1-OBu**<sup>2+</sup> are paramagnetic. The dications and the tetracation of macrocycle **3-H** display intense (dications) or weak (**3-H**<sup>4+</sup>) EPR signals. Quantum chemical calculations indicate that the four most stable conformers of the macrocycles are largely devoid of strain. Bond parameters, energies as well as charge and spin density distributions of model macrocycle **5-H**<sup>Me</sup> were calculated for the different charge and spin states.

## Introduction

Coordination cages are defined as closed structures with metal atoms as the corners and bridging ligands, the so-called linkers, as the sides. A broad variety of different architectures with various levels of complexity have meanwhile been realized, including planar polygons, three-dimensional prismatic or polyhedral cage structures, and assemblies of interlinked cages.<sup>[1]</sup> Apart from the appealing beauty of such structures, coordination cages have found use as hosts for guest binding<sup>[1,2]</sup> with applications in sensing<sup>[3]</sup> or as capsules for controlled guest re-

lease for the prospect of drug delivery,<sup>[4]</sup> as bioactive compounds,<sup>[2b,5]</sup> or as miniaturized reaction vessels for stoichiometric or catalytic transformations<sup>[2a]</sup> such as stereoselective Diels-Alder reactions or [2+2] photodimerizations.<sup>[6]</sup> The most common and simple kinds of coordination cages are rectangular structures (or tetrametallamacrocycles) comprising four metal centers with two different ditopic linkers as the sides. They are typically constructed from ligand-bridged dimetal complexes and equimolar amounts of another type of bridging, ditopic ligand of suitable topology as the individual sides in a rather predictable "self-assembly" process.

Given that a large variety of such metallamacrocycles comprises redox-active transition metal co-ligand fragments as corners and redox-active ligands as linkers it is rather surprising that the number of studies that specifically aim at capitalizing on that inherent property are rather limited. Possible perspectives such as triggering changes in guest binding inside the cavities of coordination cages or of their catalytic properties, of the optical and magnetic properties of such compounds, or of studying intracage charge-transfer phenomena through bond or through space have only occasionally been touched on. Particularly instructive examples for the latter stem from the beautiful work of Hupp and co-workers who studied the efficacy of charge transfer between diimine or porphyrinic linkers in mixed-valent tetraruthenium rectangles showing ligand-based redox activity.<sup>[7]</sup> These authors uncovered the entire continuum between a uniform distribution of charge and spin densities over both ligands, as it is characteristic of a mixed-valent

[a] S. Scheerer, Dr. M. Linseis, Dr. E. Wuttke, S. Weickert, Prof. Dr. M. Drescher, Prof. Dr. R. F. Winter

Fachbereich Chemie, Universität Konstanz  
Universitätsstraße 10, 78457 Konstanz (Germany)  
E mail: Rainer.Winter@uni-konstanz.de

[b] Dr. O. Tröppner, Prof. Dr. I. Ivanović Burmazović  
Department of Chemistry and Pharmacy  
Friedrich Alexander Universität Erlangen Nürnberg  
Egerlandstraße 1, 91058 Erlangen (Germany)

[c] A. Irmeler, Prof. Dr. F. Pauly  
Fachbereich Physik, Universität Konstanz  
Universitätsstraße 10, 78457 Konstanz (Germany)  
E mail: fabian.pauly@uni-konstanz.de

[d] Dr. E. Wuttke  
Present address: Boehringer Ingelheim Pharma GmbH & CO. KG  
Birkendorfer Straße 65, 88397 Biberach a. d. Riß (Germany)

system of Class III with a fully delocalized electronic ground state,<sup>[8]</sup> down to the limit of moderately to weakly coupled systems of Class II with dominant charge and spin localization on one redox-active ligand. The strength of interligand electronic coupling within these cages was found to depend on the spatial through-space separation of the redox-active ligands and the extent of co-facial overlap of their  $\pi$ -systems. Similar studies have been reported by Kaim, Stang and others on tetraplatinum or tetrarhenium macrocycles with oxidizable or reducible linkers.<sup>[5b,9]</sup>

We have embarked on a program which aims at utilizing well-defined, redox-active coordination cages as building blocks for the construction of anisotropic, extended 1D-, 2D- and 3D-structures. The latter would differ from classical metal-organic frameworks (MOFs)<sup>[10]</sup> in that they open the prospect of using up to three different kinds of linkers or association motifs in their 3D assembly and of encoding anisotropy already in their molecular building blocks. To these ends the individual building blocks need to offer appropriate functional groups exposed at their periphery that allow for their further association through the formation of coordinative bonds or polyaddition or -condensation reactions with suitable di- or polytopic partners. As the individual building blocks we wished to utilize metallamacrocycles constructed from 1,4-divinylphenylene-bridged diruthenium complexes of the type  $\{\text{Ru}(\text{CO})(\text{P}i\text{Pr}_3)_2(\text{X})\}_2(\mu\text{-}1,4\text{-CH=CH-C}_6\text{H}_2\text{R}_2\text{-CH=CH})$  (X = bidentate monoanionic ligand) because of their known propensity to undergo two reversible, consecutive one-electron oxidations at well-accessible potentials. Moreover, their radical cations display extensive charge and spin delocalization across the entire metal-bridge-metal backbone, which can conveniently be interrogated by means of IR and EPR spectroscopy.<sup>[11]</sup> A further interesting asset of this type of compound is their polyelectrochromism, that is, the oxidation-state-dependent absorption profiles of the three different, separately addressable states. Hence, their neutral forms are virtually transparent at wavelengths above 580 nm (X = terminal anionic ligand) or 400 nm (X = bidentate monoanionic ligand), while their radical cations exhibit intense absorptions in the visible (Vis) and deep in the near infrared (NIR). The corresponding dications finally absorb strongly at the borderline between the Vis and the NIR.<sup>[11d,f,h,m,n,12]</sup> It was our hope that coordination cages or metallamacrocycles comprising such entities and more complex architectures resulting from their ordered assembly would maintain or even amplify the favorable properties of these building blocks with the added prospect of paramagnetic behavior in states where the individual divinylphenylene-bridged diruthenium sides exist in open-shell electron configurations. Furthermore, we were interested to study the aspect of intracage electronic coupling between identical, yet differently charged sides in their mixed-valent radical cations (one side oxidized, one in the neutral state) and trications (one side doubly oxidized, one singly oxidized). As the "short" sides of the envisioned metallamacrocycles we chose benzene-1,3- or pyridine-3,5-dicarboxylates as they provide the right spatial arrangement of the chelating carboxylate donors to generate closed cyclic structures and offer an easy means to introduce addi-

tional functionalities to subsequently link individual cages to larger arrays. Furthermore, carboxylates can easily replace the chloro ligands from  $\text{Ru}(\text{CO})\text{Cl}(\text{P}i\text{Pr}_3)_2(\text{CH=CHR})$  precursors and provide a stable coordination towards the alkenyl ruthenium entity while avoiding the problem of formation of different isomers (*cis* or *trans* with respect to the placement of the carbonyl and the alkenyl ligand in the equatorial plane)<sup>[13]</sup> owing to their symmetry.<sup>[11h,14]</sup>

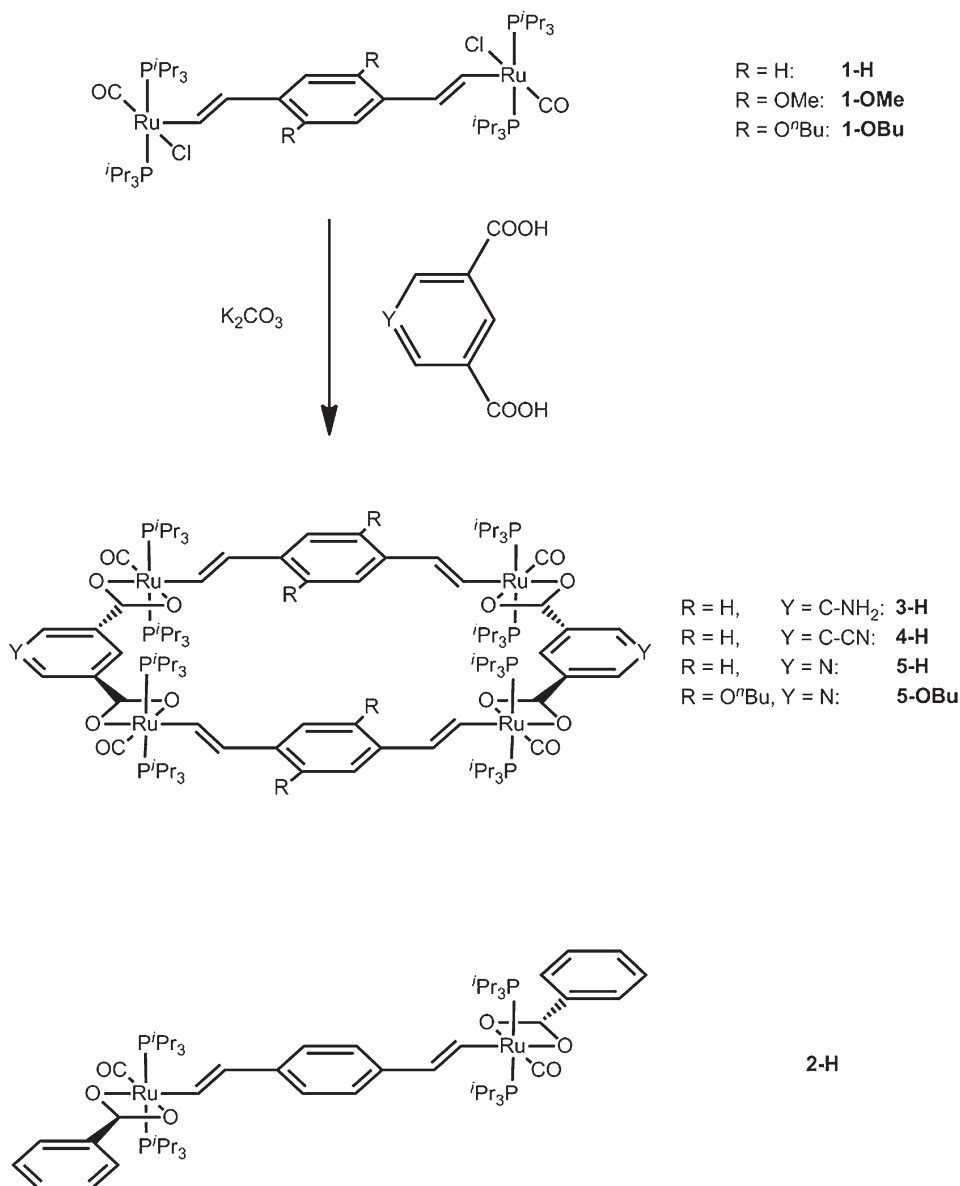
We here report on the successful conversion of 1,4-divinylphenylene-bridged diruthenium complexes including a new, even more electron-rich representative into tetraruthenium macrocycles by treatment with various arene dicarboxylate linkers and their electrochemical, structural and electronic properties along with the results of quantum chemical studies on their various redox states. It will be revealed that the moderate redox splitting for the  $+/2+/0/+$  and the  $3+/4+/2+/3+$  redox processes ( $\Delta E_{1/2}^{+/2+/0/+}$  and  $\Delta E_{1/2}^{3+/4+/2+/3+}$ ) observed in a medium of low ion pairing capability is of purely electrostatic nature and that the individual cages display well-defined three-step electrochromism with strong absorbances at low energies. We also report on the unexpected paramagnetism of dioxidized 1,4-divinylphenylene-bridged diruthenium complexes and of the di- and tetracations of the macrocyclic compounds as revealed by EPR spectroscopy at variable temperatures. The shapes and possible conformations as well as the electronic structures of these complexes and the charge and spin density distributions of their oxidized forms have been explored by quantum chemical calculations and aid in rationalizing our experimental observations.

## Results and Discussion

### Synthesis and characterization

The known 1,4-divinylphenylene-bridged diruthenium complex **1-H**<sup>[1a,b]</sup> and its more electron-rich 2,5-dimethoxy- and 2,5-dibutoxy-substituted analogues **1-OMe** and **1-OBu** in Scheme 1 are easily synthesized by the double hydorruthenation of the respective parent dialkyne with 2 equiv of  $\text{HRu}(\text{CO})\text{Cl}(\text{P}i\text{Pr}_3)_2$ .<sup>[15]</sup> The new diruthenium complex **1-OBu** offers much higher solubilities in aromatic and chlorinated hydrocarbons than poorly soluble **1-H** or **1-OMe** and was duly characterized by multinuclear NMR and IR spectroscopies (see the Experimental Section in the Supporting Information). Considering the extensive degree of electron delocalization along the  $\pi$ -conjugated {Ru}-bridge-{Ru} backbone ({Ru} =  $\text{Ru}(\text{CO})\text{Cl}(\text{P}i\text{Pr}_3)_2$  or  $\text{Ru}(\text{CO})(\text{P}i\text{Pr}_3)_2(\kappa^2\text{O},\text{O}'\text{-OOCR})$ ) it is somewhat surprising that the electron-donating OBU substituents have no noticeable effect on the position of the Ru(CO) band. Similar observations have, however, been reported by Liu and his co-workers on closely related diruthenium complexes with  $\text{Ru}(\text{CO})\text{Cl}(\text{PMe}_3)_3$  as the termini<sup>[11k]</sup> and for **1-OMe**.<sup>[16]</sup>

Single crystals of complex **1-OBu** as the solvent-free form and as the  $\text{CHCl}_3$  solvate **1-OBu·2CHCl<sub>3</sub>** were obtained by careful layering of a concentrated solution of the complex in  $\text{CH}_2\text{Cl}_2$  with *n*-hexane or from slow diffusion of *n*-pentane into a saturated solution of **1-OBu** in  $\text{CHCl}_3$  and were investigated



**Scheme 1.**

by X-ray crystallography. The molecular structure of unsolvated **1-OBu** in the solid state is shown in Figure 1 while the most pertinent bond parameters of **1-OBu** and of **1-OBu**·2CHCl<sub>3</sub> are provided in Table 1 along with those of **1-H** and closely related **1-OMe**.<sup>[16]</sup> Diffraction data and details to the structure solution and refinement are provided as Table S1 in the Supporting Information.

The Ru atoms adopt their usual square-pyramidal coordination geometry with the alkenyl ligand in the apical position, a mutual *trans* arrangement of the bulky phosphines and of the  $\sigma$ - and  $\pi$ -donating chloro and the  $\pi$ -accepting carbonyl ligand and a displacement of the Ru atom from the basal coordination plane towards the apical alkenyl ligand by 0.16 Å. The Ru-C(CO), Ru-Cl, Ru-P as well as the Ru-C(alkenyl) bond lengths present no peculiarities with respect to other complexes {Ru}CH=CHR of the Ru(CO)Cl(P*i*Pr<sub>3</sub>)<sub>2</sub> moiety.<sup>[11h,12c,d,13,16,17]</sup> The Ru

Cl...H CCl<sub>3</sub> interaction of 2.606 Å in **1-OBu**·2CHCl<sub>3</sub> is 0.344 Å shorter than the sum of the van der Waals radii, suggesting a strong hydrogen bond, but has no noticeable effect on the Ru-Cl bond length and other bond parameters in the immediate vicinity of the coordination centers. The bulky OBU substituents induce a somewhat stronger than usual rotation of the plane of the bridging divinylphenylene ligand with respect to the Ru(CO)ClCH= plane as is evident from the angle  $\phi$  between the plane defined by the phenylene unit and the *ipso*-CH atoms and that defined by the Ru(CO)Cl(C1) atoms, respectively (see the front view at the right of Figure 1). This may diminish overlap between the respective Ru d $\pi$ -orbital and the  $\pi$ -conjugated backbone of the 1,4-divinylphenylene bridge somewhat, although rotation around the Ru-vinyl bond is rapid in solution. That torsion is even larger in the chloroform solvate, obviously as a consequence of the increased steric hin-

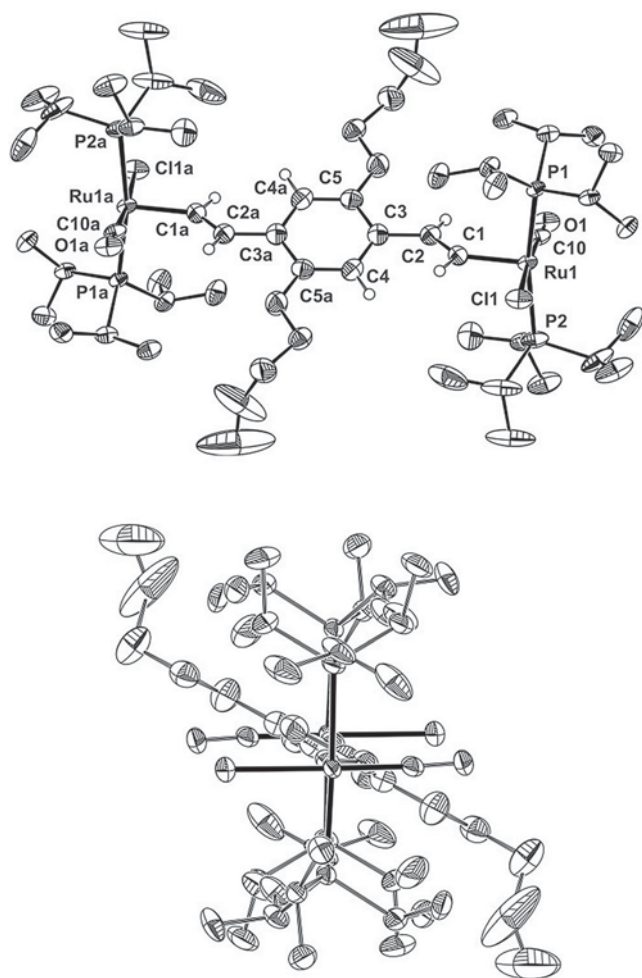


**Figure 1.** Molecular structure of complex **1 OBU** (solvent free form) in the crystal; bottom: projection along the Ru...Ru vector. Ellipsoids are at the 50% probability level.

drance imposed by the proximity of the hydrogen-bonded  $\text{CHCl}_3$  molecules to the butoxy side-chains.

Inspection of the structures of carboxylate complexes  $\text{Ru}(\text{CO})\text{Cl}(\text{PiPr}_3)_2(\kappa^2\text{O},\text{O}'\text{-OOCR})^{[11\text{h}, 14\text{a-d,g,h}]}$  suggested that benzene-1,3-dicarboxylate and pyridine-3,5-dicarboxylate linkers should be well-suited to forge two such sides into macrocyclic structures. Indeed, pure complexes **3-H** to **5-H** having the desired structures (Scheme 1) were obtained as powdery yellow to yellow-orange solids on addition of a methanolic solution of deprotonated ( $\text{K}_2\text{CO}_3$ ) aniline-3,5-dicarboxylic acid, 3,5-dicarboxybenzotrile or pyridine-3,5-dicarboxylic acid to a solution of complex **1-H** in  $\text{CH}_2\text{Cl}_2$  in yields of 25 to 37% after appropriate workup. **5-OBu** was similarly obtained from **1-OBu** and pyridine-3,5-dicarboxylic acid (Scheme 1). Combining **1-OBu** with the other dicarboxylic acids or of **1-H** and **1-OBu** with simple benzene dicarboxylic acid resulted in the formation of mixtures of macrocyclic tetra- and hexaruthenium complexes as indicated by high resolution electron spray ionization mass spectrometry (HR ESI-MS), from which no pure compounds could be isolated. In all reactions, the presence of insoluble material suggests that coordination oligomers or polymers are formed as byproducts.

Experimental proof of the identity and purity of the metallamacrocycles comes from HR ESI-MS and  $^{31}\text{P}$ ,  $^1\text{H}$  and  $^{13}\text{C}$  NMR spectroscopy. In the ESI-MS, the molecular ion peaks as well as fragment peaks derived from the loss of one or more  $\text{PiPr}_3$  ligands are observed. This is exemplarily shown in Figure 2 for **5-H**; spectra of the other compounds are collected as Figures S19–S22 in the Supporting Information. Most notably, even more intense peaks were observed for the doubly charged dications and corresponding daughter peaks resulting from the stepwise loss of up to five  $\text{PiPr}_3$  ligands with the highest intensity for the  $[\text{M} - 2\text{PiPr}_3]^{2+}$  ions. This already indicates that these cages are easily oxidized by more than just one electron. The purity of the tetraruthenium cages is indicated by the absence of any other peak assignable to hexanuclear or higher nucleari-

**Table 1.** Comparison of the most pertinent bond parameters of complexes **1 H**, **1 OMe** and of **1 OBU** in its solvent free form or as the chloroform solvate.

	<b>1 H</b>	<b>1 OBU</b>	<b>1 OBU·2CHCl<sub>3</sub></b>	<b>1 OMe</b>
Ru C(CO)	1.791(3)	1.813(4)	1.813(3)	1.7956(11)
Ru C1	1.973(2)	1.995(4)	1.996(3)	2.002(6)
Ru Cl	2.4168(9)	2.4270(10)	2.4297(9)	2.4200(18)
Ru P1	2.3805(10)	2.3972(15)	2.3965(10)	2.4009(17)
Ru P2	2.3804(11)	2.4091(16)	2.4067(10)	2.4036(16)
C1 C2	1.319(4)	1.335(5)	1.338(5)	1.332(8)
C2 C3	1.464(3)	1.481(5)	1.473(5)	1.482(8)
$d_{\text{Ru}}^{[a]}$	0.163	0.160	0.194	0.235
Ru C1 C2	134.8(2)	136.7(3)	133.7(3)	133.6 (5)
C1 C2 C3	124.6(2)	123.9(4)	124.8(3)	124.6(2)
P2 Ru P1	171.30(2)	168.47(4)	169.47(3)	171.30(2)
torsion (C1, C2, C3, C4)	160.1(3)	156.0(4)	156.3(3)	158.8(6)
torsion (C1, C2, C3, C5)	19.0(4)	24.9(6)	25.4(5)	20(1)
$\chi$ ((Ru,CO,Cl); (C3, C4, C5))	23.39	31.39	39.67	26.82
$\phi^{[b]}$	22.6	31.2	38.8	26.9
$\chi$ ((Ru,CO,Cl); (C1, C2, C3))	7.15	13.33	17.94	6.0

[a] Displacement of the Ru atom with respect to the coordination plane. [b] Angle between the planes of the phenylene unit and the immediately attached vinylic carbon atoms and that of the  $\text{Ru}(\text{CO})\text{Cl}(\text{C}=\text{C})$  unit.

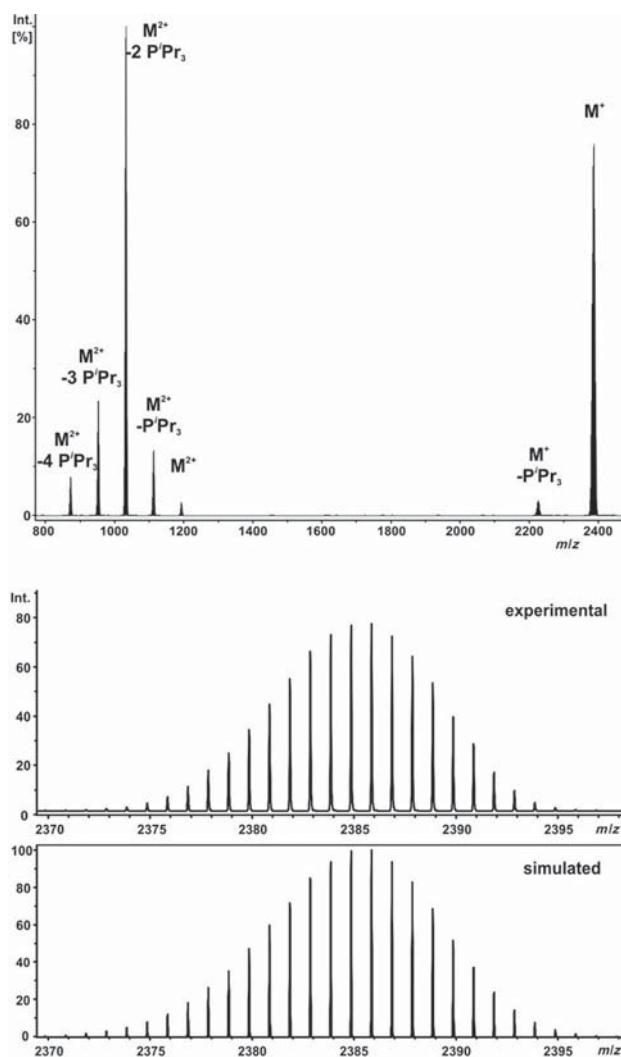


Figure 2. High resolution ESI MS spectrum of complex 5 H.

ty structures and by their  $^{31}\text{P}$  and  $^1\text{H}$  NMR spectra, where only one singlet ( $^{31}\text{P}\{^1\text{H}\}$ ) and only one set of resonance signals for the alkenyl and the chemically equivalent protons or carbon atoms of the divinylphenylene and dicarboxylate linkers ( $^1\text{H}$ ) are observed (Figures S1–S18 in the Supporting Information). Mixtures of different macrocyclic structures obtained in other

cases gave individual and distinguishable sets of NMR resonances for every different species. As usual, chloride substitution by a bidentate carboxylate ligand induces low-field shifts of the alkenyl protons, a modest high-field shift of the  $^{31}\text{P}$  NMR resonance and diminishes the energy of the Ru–CO stretch by 6 to  $8\text{ cm}^{-1}$  as the metal ions attain 18 valence-electron (VE) configurations.

### Electrochemistry

Like **1-H** and **1-OMe**, diruthenium precursor **1-OBu** undergoes two consecutive one-electron oxidations. The half-wave potentials of 246 and 54 mV in the  $\text{CH}_2\text{Cl}_2/\text{NBu}_4^+\text{PF}_6^-$  (0.1 M) electrolyte are slightly lower (less anodic) than those of **1-OMe** and more appreciably so than those of **1-H** (Table 2). In the less ion-pairing  $\text{CH}_2\text{Cl}_2/\text{NBu}_4^+\text{B}\{\text{C}_6\text{H}_3(\text{CF}_3)_2\text{-3,5}\}_4^-$  (0.1 M) supporting electrolyte a drift of particularly the first oxidation potential to lower values and, accordingly, a larger half-wave potential splitting  $\Delta E_{1/2}$  of 333 mV are observed. The same also holds for **1-H**, where  $\Delta E_{1/2}$  increases from 250 mV in  $\text{CH}_2\text{Cl}_2/\text{NBu}_4^+\text{PF}_6^-$  to 308 mV in  $\text{CH}_2\text{Cl}_2/\text{NBu}_4^+\text{B}\{\text{C}_6\text{H}_3(\text{CF}_3)_2\text{-3,5}\}_4^-$ . The dependence of  $\Delta E_{1/2}$  on the counterion of the supporting electrolyte reflects the well-known fact that higher charge states are comparatively more stabilized by ion pairing than lower ones.<sup>[18]</sup>

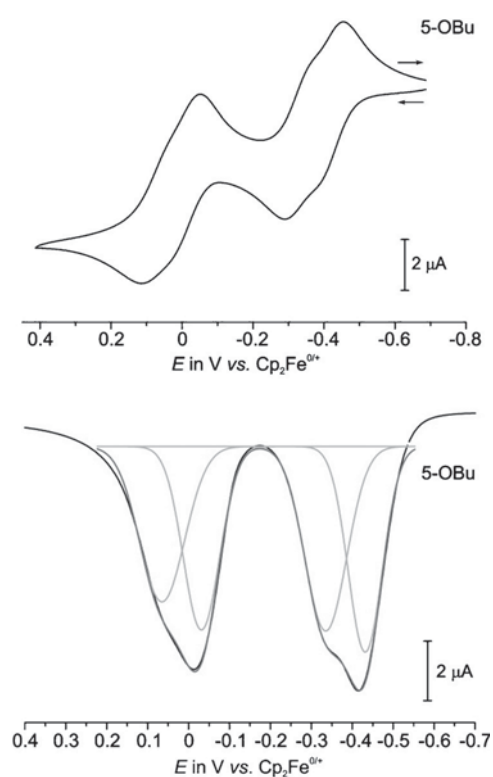
Chloride substitution by bidentate benzoate ligands and the concomitant increase of the valence electron count from 16 to 18 stabilizes the various oxidized forms as it is, for example, evident from the sizable cathodic displacement of both half-wave potentials in **2-H** when compared to **1-H**.<sup>[11h]</sup> The same effect is also seen in the rectangular tetra-ruthenium macrocycles **3-H** to **5-H** and **5-OBu** (Table 2). In the  $\text{CH}_2\text{Cl}_2/\text{NBu}_4^+\text{PF}_6^-$  supporting electrolyte all tetra-ruthenium macrocycles are oxidized in two consecutive and chemically reversible but slightly broadened waves, indicating that the first and the second oxidations of each individual 1,4-divinylphenylene diruthenium subunit are not resolved. In the even less ion-pairing  $\text{CH}_2\text{Cl}_2/\text{NBu}_4^+\text{B}\{\text{C}_6\text{H}_3(\text{CF}_3)_2\text{-3,5}\}_4^-$  electrolyte, however, the first, and in the case of **5-H** and **5-OBu**, also the second composite waves are split into two closely spaced, consecutive one-electron processes with half-wave potential differences between the  $+2/+$  and the  $0/+$  processes ( $\Delta E_{1/2}^{+2/+//0/+}$ ) or the  $3+/4+$  and the  $2+/3+$  processes ( $\Delta E_{1/2}^{3+/4+//2+/3+}$ ) in the range of 60 to

Table 2. Electrochemical data<sup>[a,b]</sup> for all complexes.

Complex	$\text{NBu}_4^+\text{X}^{[b]}$	$E_{1/2}$ (0/+)	$E_{1/2}$ (+2/+)	$E_{1/2}$ (2+/3+)	$E_{1/2}$ (3+/4+)	$\Delta E_{1/2}$ (+2/+//0/+)	$\Delta E_{1/2}$ (2+/3+//+2/+)	$\Delta E_{1/2}$ (3+/4+//2+/3+)
<b>1 H</b>	$\text{PF}_6^-$	75	175			250		
	BArF	180	128			308		
<b>1 OMe</b> <sup>[c]</sup>	$\text{PF}_6^-$	215	60			275		
	$\text{PF}_6^-$	246	54			300		
<b>1 OBu</b>	BArF	330	3			333		
	BArF	384	304	22	22	80	326	
<b>4 H</b>	BArF	308	230	91	91	78	321	
<b>5 H</b>	BArF	320	229	78	140	91	307	62
<b>5 OBu</b>	BArF	431	334	39	42	97	295	81

[a] All potentials in mV ( $\pm 3$  mV) in  $\text{CH}_2\text{Cl}_2$  at  $T=293(\pm 3)$  K relative to the  $\text{Cp}_2\text{Fe}^{0/+}$  couple ( $E_{1/2}=0.000$  V). [b] BArF =  $\text{B}\{\text{C}_6\text{H}_3(\text{CF}_3)_2\text{-3,5}\}_4^-$ . [c] From reference [16].

100 mV as derived from deconvolution of the square wave peaks by Gaussian shaped functions. Representative cyclic and square wave voltammograms of **5-OBu** are displayed in Figure 3 while those for the other compounds are collected in the Supporting Information (Figures S23–S31).



**Figure 3.** Comparison of cyclic ( $\nu = 100 \text{ mV s}^{-1}$ ) and square wave voltammograms (step height 4 mV, pulse width 4 mV, frequency = 25 Hz) of **5-OBu** in  $\text{CH}_2\text{Cl}_2$  at  $T = 293(\pm 3) \text{ K}$  with the  $0.1 \text{ M NBu}_4^+ \text{B}\{\text{C}_6\text{H}_3(\text{CF}_3)_2\}_4^-$  electrolyte.

As seen by the data in Table 2 individual half-wave potentials  $E_{1/2}$  respond to the electronic properties of the 1,4-divinylphenylene (c.f. **5-H** vs. **5-OBu**) and also to those of the dicarboxylate linkers (compare **3-H**, **4-H**, **5-H**). While the influence of the alkoxy substituents at the divinylphenylene ligand is readily explained by strong contributions of the nominal bridge to the so-called “redox orbitals” HOMO and HOMO 1,<sup>[11a–c,f,h,k,m,n,12c,d,19]</sup> that of dicarboxylate linkers is likely of an inductive origin as carboxylate ligands do generally not contribute to the frontier MOs of such alkenyl ruthenium complexes.<sup>[11h,14f]</sup>

The redox splittings observed between the  $+2/+$  and the  $0/+$  redox couples of all tetraruthenium macrocycles and between the  $3+/4+$  and the  $2+/3+$  couples of compounds **5-H** and **5-OBu** raise the question of the relevance of electronic (or “resonance”) interactions through bond or through space *between* the individual sides in the mixed-valent states as it was observed in Hupp’s tetraruthenium rectangles.<sup>[7]</sup> As a matter of fact, some conjugated bis(alkenyl)-bridged diruthenium complexes closely related to the precursor **1-H** have been proven to exhibit appreciable degrees of ground-state delocali-

zation of their mixed-valent radical cations despite only moderate or even small half-wave potential splittings close to the statistical limit.<sup>[11f]</sup> While through-space interactions between the individual styryl decks of alkenyl ruthenium-appended [2,2]paracyclophanes were established,<sup>[17f]</sup> the redox splitting of 112 mV, observed for their ferrocenyl-appended counterparts, was found to be of purely electrostatic origin.<sup>[20]</sup> We also note here that the often-purported direct relation between half-wave potential splittings and resonance interactions stands on shaky ground, particularly when the nominal redox site is not strictly confined to the termini of an overall two-step redox system comprising two interconnected redox-active subunits.<sup>[11g,21]</sup>

### IR and UV/Vis/NIR spectroelectrochemistry

In order to address that issue and to also establish the degree of electronic coupling *within* each 1,4-divinylphenylene diruthenium side, IR and UV/Vis/NIR (NIR = near infrared) spectroelectrochemical (SEC) experiments were performed with divinylphenylene-bridged diruthenium complexes **1-H**, **1-OMe**, **1-OBu** and **2-H** as reference points. The results of such an in situ electrolysis experiment on **1-OBu** conducted under IR monitoring inside an optically transparent thin-layer cell<sup>[22]</sup> are shown as Figures S32 and S35 in the Supporting Information. Thus, on gradual oxidation to its radical cation, the Ru(CO) band of neutral **1-OBu** at  $1911 \text{ cm}^{-1}$  is replaced by a slightly asymmetric band which can be deconvoluted into two closely spaced Gaussian bands peaking at  $1932$  and  $1935 \text{ cm}^{-1}$ . According to DFT calculations this splitting arises rather from a non-degeneracy of the symmetric and antisymmetric combinations of the individual Ru(CO) stretches than from intrinsically different electron densities at the individual {Ru} sites. On further oxidation to the dication **1-OBu**<sup>2+</sup> the Ru(CO) band experiences a further blue-shift to  $1972 \text{ cm}^{-1}$  with no noticeable splitting between the symmetric and non-symmetric combinations. The overall band shift of  $61 \text{ cm}^{-1}$  on twofold oxidation is virtually identical to that of **1-OMe** but appreciably smaller than that of  $68 \text{ cm}^{-1}$  for **1-H**,<sup>[16]</sup> in line with enhanced contributions of the more electron-rich divinylphenylene entity to the “redox orbitals”. Very similar results are observed for the bis(-benzoato) complex **2-H** (Table 3 and Figure 4), only that the Ru(CO) band positions of **2-H**<sup>n+</sup> are lowered by about  $7 \text{ cm}^{-1}$  with respect to **1-H**<sup>n+</sup> as a consequence of the higher valence electron count at the metal (18 versus 16 in the neutral state). A further peculiarity is a notable asymmetry of the Ru(CO) band at any oxidation state. In that particular case, that splitting is therefore no token of an electronically asymmetric ground-state configuration of mixed-valent **2-H**<sup>+</sup> but more likely related to the presence of several rotamers with various degrees of metal versus bridge contributions to the SOMO and various degrees of  $\pi$ -conjugation across the 1,4-divinylphenylene diruthenium backbone as it has already been documented for closely related systems.<sup>[23]</sup> Relative metal/bridging ligand contributions to the redox orbitals critically depend on the torsions around the Ru alkenyl and the alkenyl arylene bonds. The formation of the radical cations **1-OBu**<sup>+</sup> and **2-H**<sup>+</sup> is also

Table 3. IR data of the complexes in their various oxidation states.		
	$\nu(\text{CO})$	$\nu_{\text{C-C}}$ (alkenyl, aryl)
1 OBU <sup>[b]</sup>	1911	1559
1 OBU <sup>+</sup> [b]	1932, 1935	1486, 1490
1 OBU <sup>2+</sup> [b]	1972	1498, 1532
2 H <sup>[b]</sup>	1904	1531
2 H <sup>+</sup> [b]	1924	1518, 1503, 1481
2 H <sup>2+</sup> [b]	1971	1519
3 H <sup>[a]</sup>	1902	1534, 1573
3 H <sup>2+</sup> [a]	1926, 1942	1445, 1505, 1527
3 H <sup>4+</sup> [a]	1979	1469, 1521
4 H <sup>[c]</sup>	1904	1533, 1551, 1573
4 H <sup>2+</sup> [c]	1930, 1946	1445, 1504, 1528
4 H <sup>4+</sup> [c]	1973, 1987	1520
5 H <sup>[b]</sup>	1904	1533, 1574
5 H <sup>2+</sup> [b]	1930, 1945	1505, 1529
5 H <sup>4+</sup> [b]	1980	1521
5 OBU <sup>[a]</sup>	1902	1596
5 OBU <sup>2+</sup> [a]	1930, 1942	1468, 1478, 1510, 1593
5 OBU <sup>4+</sup> [a]	1978	1499, 1526, 1590

[a] In CH<sub>2</sub>Cl<sub>2</sub>/0.25 M NBu<sub>4</sub><sup>+</sup>B{C<sub>6</sub>H<sub>3</sub>(CF<sub>3</sub>)<sub>2</sub> 3,5}<sub>4</sub> at 293 (±3) K. [b] In 1,2-C<sub>2</sub>H<sub>4</sub>Cl<sub>2</sub>/0.25 M NBu<sub>4</sub><sup>+</sup>PF<sub>6</sub><sup>-</sup> at 293(±3) K. [c] In CH<sub>2</sub>Cl<sub>2</sub>/0.25 M NBu<sub>4</sub><sup>+</sup>PF<sub>6</sub><sup>-</sup> at 293(±3) K.

accompanied by the development of a highly intense electronic transition at about 7500 cm<sup>-1</sup> (1330 nm) resulting from a  $\pi \rightarrow \pi^*$  SOMO 1  $\rightarrow$  SOMO ( $\beta$ -HOSO  $\rightarrow$   $\beta$ -LUSO) transition

within the open-shell diruthenium divinylphenylene chromophore.<sup>[11a-c,f,h,m,n,19]</sup> This band bleaches on further oxidation to the corresponding dications.

The responses of the tetraruthenium macrocycles **3-H**, **4-H**, **5-H** and **5-OBu** to IR SEC experiments are essentially identical to those of the diruthenium bis(benzoato) complex **2-H**, irrespective of whether PF<sub>6</sub><sup>-</sup> or B{C<sub>6</sub>H<sub>3</sub>(CF<sub>3</sub>)<sub>2</sub> 3,5}<sub>4</sub><sup>-</sup> (BARF<sup>-</sup>) are employed as the supporting electrolyte counterion (as a matter of fact, the latter is preferably used due to the higher solubilities of the di- and tetracations with that particular counterion). On slowly scanning the first composite wave comprising the +/2+ and 0/+ couples, a structured Ru(CO) band peaking at about 1930 cm<sup>-1</sup> with a well-defined shoulder to higher energies develops along with other bridge-based absorptions and the typical NIR band at about 7800 cm<sup>-1</sup>. As further oxidation to the tetracations proceeds, the Ru(CO) bands of the dications give way to a similarly structured, shifted absorption at about 1980 cm<sup>-1</sup> along with a bleach of the bridge stretching and bending modes and of the prominent NIR band. This is exemplarily shown in Figure 5 for complex **5-OBu**; graphical representations of the results for the other cage compounds are provided as Figures S36 to S55 in the Supporting Information. The spectra of the di- and tetracations of the tetraruthenium macrocycles are virtually superimposable to those of radical cation **2-H<sup>+</sup>** or of dication **2-H<sup>2+</sup>**, respectively, and the positions of their Ru(CO) bands in the respective oxidation states

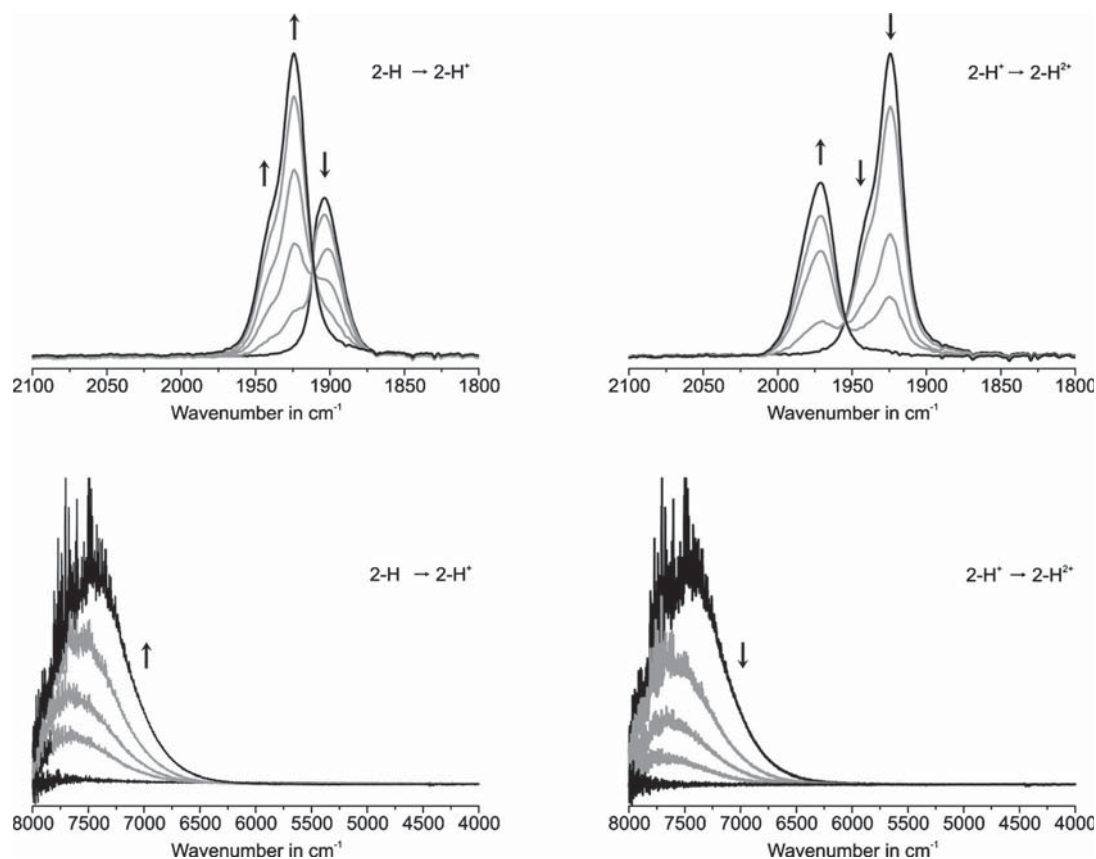
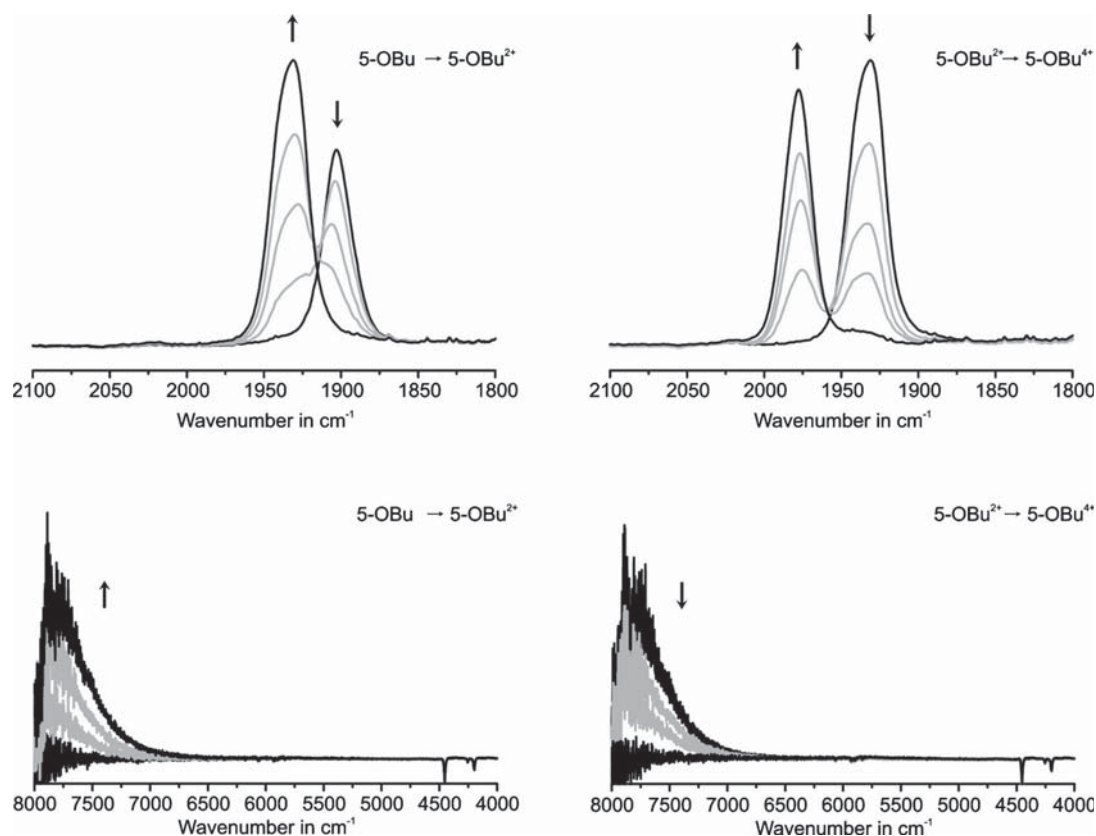


Figure 4. Changes of IR spectra of diruthenium complex **2 H** (1,2 C<sub>2</sub>H<sub>4</sub>Cl<sub>2</sub>, NBu<sub>4</sub><sup>+</sup> PF<sub>6</sub><sup>-</sup>, T=293(±3) K) in the Ru(CO) (top) and the NIR/IR (bottom) region during the first (left) and the second (right) oxidation.



**Figure 5.** Changes of IR spectra of the macrocyclic tetraruthenium complex **5 OBu** ( $\text{CH}_2\text{Cl}_2$ ,  $\text{NBu}_4^+\text{B}\{\text{C}_6\text{H}_5(\text{CF}_3)_2\}_4^-$ ,  $T=293(\pm 3)$  K) in the Ru(CO) (top) and the NIR (bottom) regions on slowly scanning the first (left) and second (right) composite two electron waves.

are hardly affected by the substituents at the phenylene bridges or the dicarboxylate linkers (Table 3).

Most importantly, the radical cations and trications have no specific IR or NIR bands. Given the half-wave potentials of Table 2 and comproportionation equilibrium constants  $K_{c1}$  and  $K_{c3}$  as defined by Equations (1) and (2), those mixed-valent species must account for at least 50% of the total amount of the compounds in solution after the passage of one or three electrons per macrocycle. This indicates that the two interconnected diruthenium 1,4-divinylphenylene sides are mutually insulated from each other and that the charge and spin densities of the intermediate radical cations or trications are delocalized *within* each diruthenium divinylphenylene subunit but not *between* the individual sides. It comes as no surprise that the dicarboxylate linkers are unable to promote through-bond resonance interactions between the sides as the carboxylate co-ligands of alkenyl ruthenium complexes  $\text{Ru}(\text{CO})(\text{P}i\text{Pr}_3)_2(\text{CH}=\text{CHR})(\kappa^2\text{O},\text{O}'\text{-OOCR}')$  essentially do not contribute to the HOMO.<sup>[11h,14f]</sup> As for the inefficacy of such interactions through space one might suppose that the stacking distance between the sides may be too large. As it will be discussed in more detail below, quantum chemical calculations point to another reason: Structure optimization of the tetraruthenium macrocycles indicates a lateral (or side-by-side) placement of the individual divinylphenylene diruthenium sides, which precludes electronic coupling through-space [Eqs. (1) and (2)]:

$$K_{c1} = [\text{A}^{+2}]^2 / ([\text{A}^{2+}] \times [\text{A}]) = \exp\{(F \times \Delta E_{1/2}^{+/2+/0/+}) / (RT)\} \quad (1)$$

$$K_{c3} = [\text{A}^{3+}]^2 / ([\text{A}^{4+}] \times [\text{A}^{2+}]) = \exp\{(F \times \Delta E_{1/2}^{3+/4+/12+/3+}) / (RT)\} \quad (2)$$

UV/Vis/NIR SEC studies fully confirm the above conclusions. Thus, spectroscopic changes observed during the overall two-electron oxidations of the neutral to the dioxidized macrocycles, where both diruthenium 1,4-divinylphenylene sides are oxidized by one electron each, are fully consistent with those observed during the 0/+ process of complexes **1-H**, **1-OMe**, **1-OBu** or **2-H**. The same holds when comparing the spectroscopic changes on further oxidation to their tetracations to those observed during the second oxidation of a 1,4-divinylphenylene-bridged diruthenium precursor. Figure 6 provides such a comparison. Again, the intermittently formed radical cations and trications have no specific absorptions within the entire régime of the electronic spectrum such that each individual spectrum recorded during the first electrolysis step is an exact overlay of that of the neutral and that of the dication and each spectrum recorded during the second composite two-electron step looks like that of a mixture of the di- and tetracations. The results of UV/Vis/NIR SEC experiments of all other compounds of this study are collected as Figures S56–S67 in the Supporting Information.

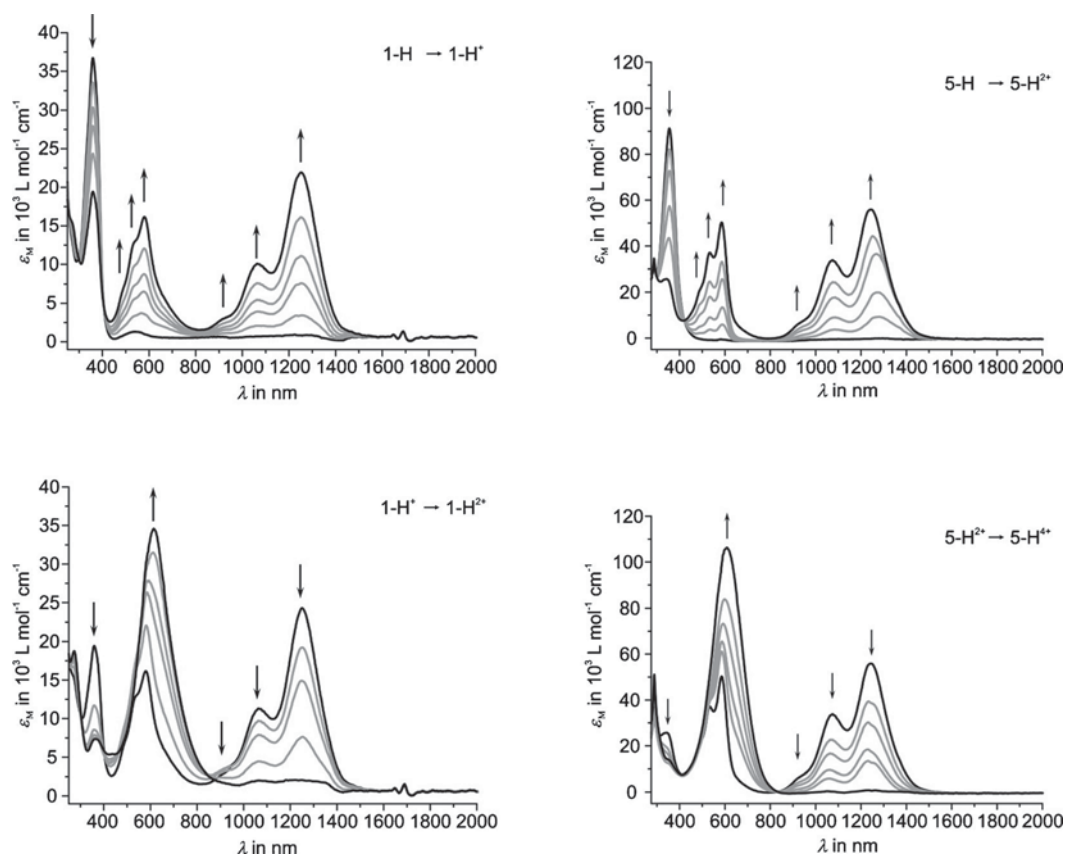


**Figure 6.** Spectroscopic changes during the first (top left) and second (bottom left) oxidation of complex **1 H** and of the oxidation of **5 H** to **5 H<sup>2+</sup>** (top right) and of **5 H<sup>2+</sup>** to **5 H<sup>4+</sup>** (bottom right) in  $\text{CH}_2\text{Cl}_2/\text{NBu}_4^+\text{PF}_6^-$  (**1 H**) or  $\text{CH}_2\text{Cl}_2/\text{NBu}_4^+\text{B}(\text{C}_6\text{H}_3(\text{CF}_3)_2)_4^-$  (**5 H**) inside an OTTE cell at  $T=293(\pm 3)$  K.

Overall, the polyelectrochromic properties (i.e., oxidation state-dependent absorption profiles) of the parent 1,4-divinylphenylene-bridged diruthenium complexes are amplified as seen by the twofold (or even larger) increase of the extinction coefficients (Table 4). Thus, extinction coefficients

reach rather impressive values of  $>6 \times 10^4 \text{ m}^{-1} \text{ cm}^{-1}$  for the NIR bands of the dications and of up to  $1.1 \times 10^5 \text{ m}^{-1} \text{ cm}^{-1}$  for the tetracations (for other accounts of highly efficient metal-organic polyelectrochromic dyes, see references [12a,b] and [24]).

**Table 4.** UV/Vis/NIR data of the complexes in their various oxidation states.

	$\lambda_{\text{max}}$ [nm] ( $\epsilon$ [ $\text{L mol}^{-1} \text{ cm}^{-1}$ ])
<b>1 OBU</b> <sup>[a]</sup>	247 (24 200), 260 (26 800), 305 (15 300), 319 (15 700), 369 (35 600), 387 (38 100), 403 (27 300), 499 (1840)
<b>1 OBU</b> <sup>+</sup> <sup>[a]</sup>	264 (20 900), 283 (17 200), 319 (9900), 375 (14 200), 396 (12 900), 483 (10 900), 540 (17 900), 605 (21 400), 633 (16 500), 992 (5700), 1151 (13 500)
<b>1 OBU</b> <sup>2+</sup> <sup>[a]</sup>	278 (20 100), 307 (11 300), 374 (8700), 460 (9600), 516 (18 900), 619 (22 700), 712 (19 700)
<b>2 H</b> <sup>[a]</sup>	362 (33 800)
<b>2 H</b> <sup>+</sup> <sup>[a]</sup>	357 (12 800), 487 (6600), 536 (6800), 587 (8000), 1016 (1200), 1084 (1900), 1272 (5800)
<b>2 H</b> <sup>2+</sup> <sup>[a]</sup>	375 (9200), 427 (9000), 606 (13 000)
<b>3 H</b> <sup>[b]</sup>	345 (86 600), 368 (83 500)
<b>3 H</b> <sup>2+</sup> <sup>[b]</sup>	310 (26 000), 346 (32 000), 506 (19 000), 538 (28 400), 589 (39 100), 992 (7900), 1092 (25 200), 1271 (43 600)
<b>3 H</b> <sup>4+</sup> <sup>[b]</sup>	354 (11 100), 495 (16 000), 585 (62 900), 625 (63 000)
<b>4 H</b> <sup>[c]</sup>	329 (58 600), 345 (78 800), 364 (79 000)
<b>4 H</b> <sup>2+</sup> <sup>[c]</sup>	330 (28 800), 362 (29 700), 433 (18 000), 497 (29 300), 538 (38 000), 588 (51 000), 952 (5600), 1086 (28 800), 1257 (49 700), 1389 (14 300)
<b>4 H</b> <sup>4+</sup> <sup>[c]</sup>	363 (21 300), 467 (34 000), 590 (69 600), 638 (60 000)
<b>5 H</b> <sup>[b]</sup>	351 (90 000), 363 (86 300)
<b>5 H</b> <sup>2+</sup> <sup>[b]</sup>	300 (26 500), 341 (25 700), 361 (22 100), 516 (19 800), 588 (50 200), 650 (6500), 975 (10 000), 1076 (33 800), 1245 (55 900)
<b>5 H</b> <sup>4+</sup> <sup>[b]</sup>	340 (14 600), 508 (31 600), 581 (94 300), 631 (10 1000)
<b>5 OBU</b> <sup>[b]</sup>	302 (35 500), 318 (40 900), 374 (76 400)
<b>5 OBU</b> <sup>2+</sup> <sup>[b]</sup>	314 (22 400), 366 (19 700), 458 (10 600), 506 (23 200), 543 (40 000), 596 (56 300), 895 (5600), 1008 (26 300), 1159 (51 600)
<b>5 OBU</b> <sup>4+</sup> <sup>[b]</sup>	360 (11 300), 555 (42 100), 632 (88 900), 687 (83 500), 748 (46 700)

[a] In  $1,2\text{-C}_2\text{H}_4\text{Cl}_2/0.25\text{ M NBu}_4^+\text{PF}_6^-$  at  $293(\pm 3)$  K. [b] In  $\text{CH}_2\text{Cl}_2/0.25\text{ M NBu}_4^+\text{B}(\text{C}_6\text{H}_3(\text{CF}_3)_2)_4^-$  at  $293(\pm 3)$  K. [c] In  $1,2\text{-C}_2\text{H}_4\text{Cl}_2/0.25\text{ M NBu}_4^+\text{PF}_6^-$  at  $293(\pm 3)$  K.

Macrocycles **3-H** to **5-OBu** were successfully oxidized with ferrocenium hexafluoroantimonate to yield persistent, intensely deep purple or blue-violet colored dicationic species. By using an excess (> 4 equiv) of acetylferrocenium hexafluoroantimonate, **3-H** could even be transformed to the moderately stable cobalt blue tetracation **3-H<sup>4+</sup>**. We note that the hexafluoroantimonate salts proved to be much more stable than the corresponding hexafluorophosphates owing to the appreciably lower tendency to decompose by the release of highly nucleophilic free fluoride ions. The oxidized samples were spectroscopically pure as judged from their IR and UV/Vis/NIR spectra.

### EPR spectroscopy

EPR spectroscopy on open-shell systems often provides useful information on the metal/ligand character of the partially occupied MO(s), the delocalization of the unpaired spin in mixed-valent compounds and on magnetic interactions between unpaired spins in multispin systems. Radical cations of 1,4-divinylphenylene-bridged diruthenium complexes or of their more extended bis(styryl)ethene-bridged counterparts generally exhibit intense EPR signals in fluid solution with resolved hyperfine splittings (hfs) to four equivalent phosphorus and two equivalent <sup>99/101</sup>Ru nuclei. This is a token of complete spin delocalization on the EPR timescale of about 10<sup>-8</sup> s.<sup>[25]</sup> Radical cations **1-OMe<sup>+</sup>**<sup>[16]</sup> and **1-OBu<sup>+</sup>** are no exceptions; the A(<sup>31</sup>P) and A(<sup>99/101</sup>Ru) hfs constants of 8.9 and 5.3 G are in the usual range (Table 5, for spectra see Figures S68–S70 in the Supporting Information).<sup>[11b,f,16]</sup> Owing to the larger number of nuclei with I ≠ 0 and the concomitant increase of the number of unresolved hfs to hydrogen atoms, signal resolution is lost in the bis(benzoato)-substituted diruthenium radical complex **2-H<sup>+</sup>** such that a broadened isotropic signal is obtained (Table 5 and Figures S71 and S72 in the Supporting Information).

The dicationic species of the macrocyclic tetra-ruthenium complexes, where both divinylphenylene diruthenium sides are oxidized

by one electron each, may be either present as EPR active triplets, EPR silent singlet diradicals, or as paramagnetic species with two non-interacting radical sites. EPR samples of the dicationic species were either generated by electrolysis inside an EPR tube or by chemical oxidation as described above. IR and UV/Vis/NIR spectra of the chemically generated samples were superimposable to those recorded after full conversion of the neutrals to their dicationic species in the SEC experiments, thus ensuring that they were not contaminated by radical cations (the latter would be formed by comproportionation of the dication with the neutral starting compounds as long as some of it is left in solution and display the spectroscopic characteristics of the neutral and the dicationic complexes owing to their non-interacting redox sites, vide infra). All dicationic species were found to be EPR active with *g*-values in a narrow range of 2.035 to 2.041, very similar to that of **2-H<sup>+</sup>** and those of precursors **1-H<sup>+</sup>**, **1-OMe<sup>+</sup>** and **1-OBu<sup>+</sup>** (Table 5). Intense EPR signals are also obtained in a frozen CH<sub>2</sub>Cl<sub>2</sub> matrix at *T* = 103 K. As shown in Figure 7 for **3-H<sup>2+</sup>** as a representative example and in the Supporting Information for all other compounds of this study (Figures S73–S78), the EPR signals notably retain their isotropic character on freezing. The increase of the valence electron count by two electrons compared to the five-coordinated precursors is therefore not accompanied by a larger anisotropy of the *g*-tensors.

Very much to our surprise, the fourfold oxidized form of the most electron-rich cage **3-H**, that is **3-H<sup>4+</sup>**, generated by treating **3-H** with excess acetylferrocenium hexafluoroantimonate to ensure complete conversion, is also EPR active in fluid and in frozen CH<sub>2</sub>Cl<sub>2</sub> solution (Figure 8). The signal intensity is, however, much lower than that of **3-H<sup>2+</sup>** at similar concentration levels. As above, the purity of the chemically generated sample of **3-H<sup>4+</sup>** was verified by the absence of the IR and UV/Vis/NIR peaks of **3-H<sup>2+</sup>**. The slightly increased *g*-value of 2.0550 when compared to that of 2.0414 for **3-H<sup>2+</sup>** may point to some limited increase in metal contributions to the relevant spin orbitals but still not to the degree of causing noticeable anisotropy of the *g*-tensor. On the other hand, the *g*-value is sufficiently different to that of **3-H<sup>2+</sup>** to exclude that the observed signal is due to residual **3-H<sup>2+</sup>**. That result implies that a paramagnetic state is partially populated even at low *T*.

This observation also raises the question of the overall spin state of the dioxidized 1,4-divinylphenylene diruthenium entities present in **3-H<sup>4+</sup>**. Common wisdom based on the spin-polarization formalism and spin topology underlying Ovchinnikov's rule<sup>[26]</sup> would clearly point to a singlet ground state.<sup>[27]</sup> Above that, previous quantum chemical calculations on **1-H<sup>2+</sup>** have placed the singlet state well below the ferromagnetically coupled triplet state.<sup>[11b]</sup> There are, however, some documented exceptions showing ferromagnetically coupled spins in the ground state, including purely organic diradicals of the same general architecture.<sup>[28]</sup> In addition, recent work has unearthed several closely related systems with open-shell singlet diradical ground states and slightly higher lying ferromagnetic triplet states, among them dicationic species of bis(triarylamine)-substituted 1,4-phenylenes and 4,4'-biphenylenes akin to Thiele's and Chi-

Complex	Charge	<i>T</i> [K]	<i>g</i> value	A( <sup>31</sup> P) (G) <sup>[b]</sup>	A( <sup>99/101</sup> Ru) (G) <sup>[b]</sup>	A( <sup>1</sup> H) (G) <sup>[b]</sup>
<b>1 H</b>	+	RT	2.0397	9.7 (4)	5.6 (2)	
<b>1 H</b>	2+	RT	2.0558	18.9 (2)	10.7 (1)	7.1 (2)
<b>1 OBU</b>	+	RT	2.0340	8.9 (4)	5.3 (2)	
<b>1 OBU</b>	+	103	2.0334			
<b>1 OBU</b>	2+	RT	2.0313	14.3 (2)	6.1 (1)	8.9 (2)
<b>1 OBU</b>	2+	103	2.0307			
<b>3 H</b>	2+	RT	2.0408			
<b>3 H</b>	2+	103	2.0414			
<b>3 H</b>	4+	RT	2.055			
<b>3 H</b>	4+	103	2.053			
<b>4 H</b>	2+	RT	2.0406			
<b>4 H</b>	2+	103	2.0370			
<b>5 H</b>	2+	RT	2.0407			
<b>5 H</b>	2+	103	2.0408			
<b>5 OBU</b>	2+	RT	2.0358			
<b>5 OBU</b>	2+	103	2.0352			

[a] In CH<sub>2</sub>Cl<sub>2</sub> solution. [b] The number of interacting nuclei is given in parentheses.

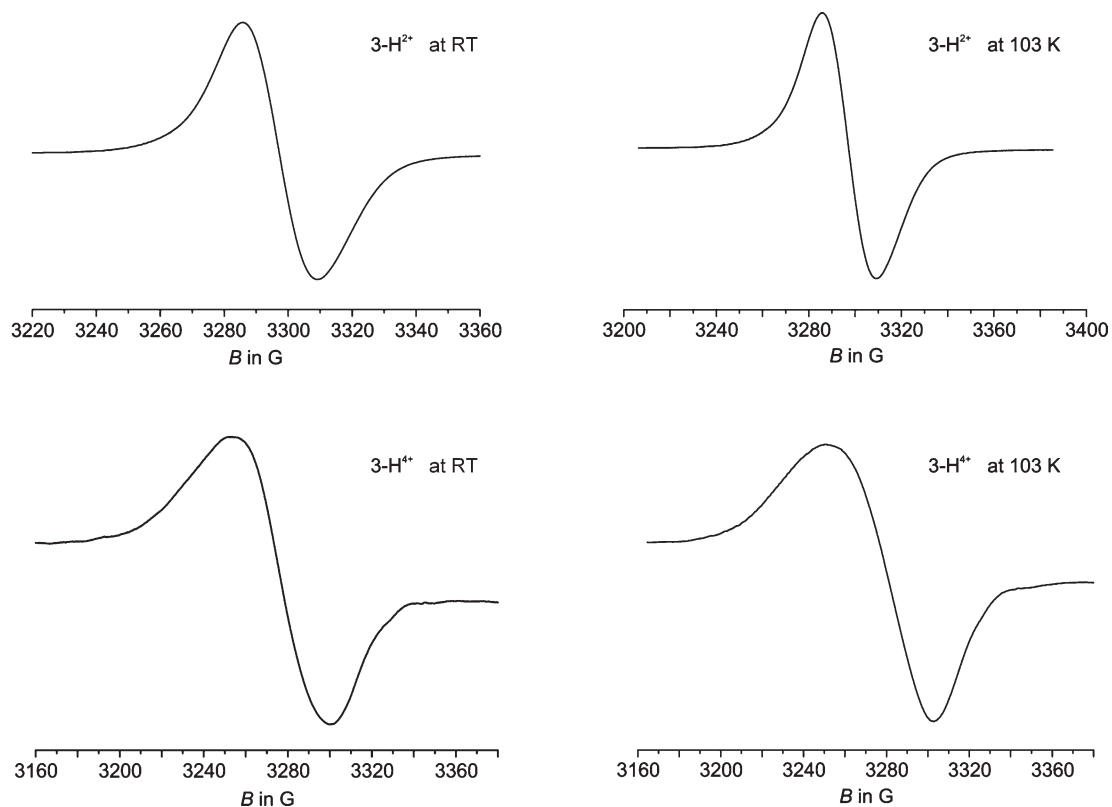


**Figure 7.** EPR spectra of  $3\text{ H}^{2+}$  in fluid solution at RT (top left) and in frozen solution at 103 K (top right) and of  $3\text{ H}^{4+}$  in fluid solution at RT (bottom left) and in frozen solution at 103 K (bottom right).

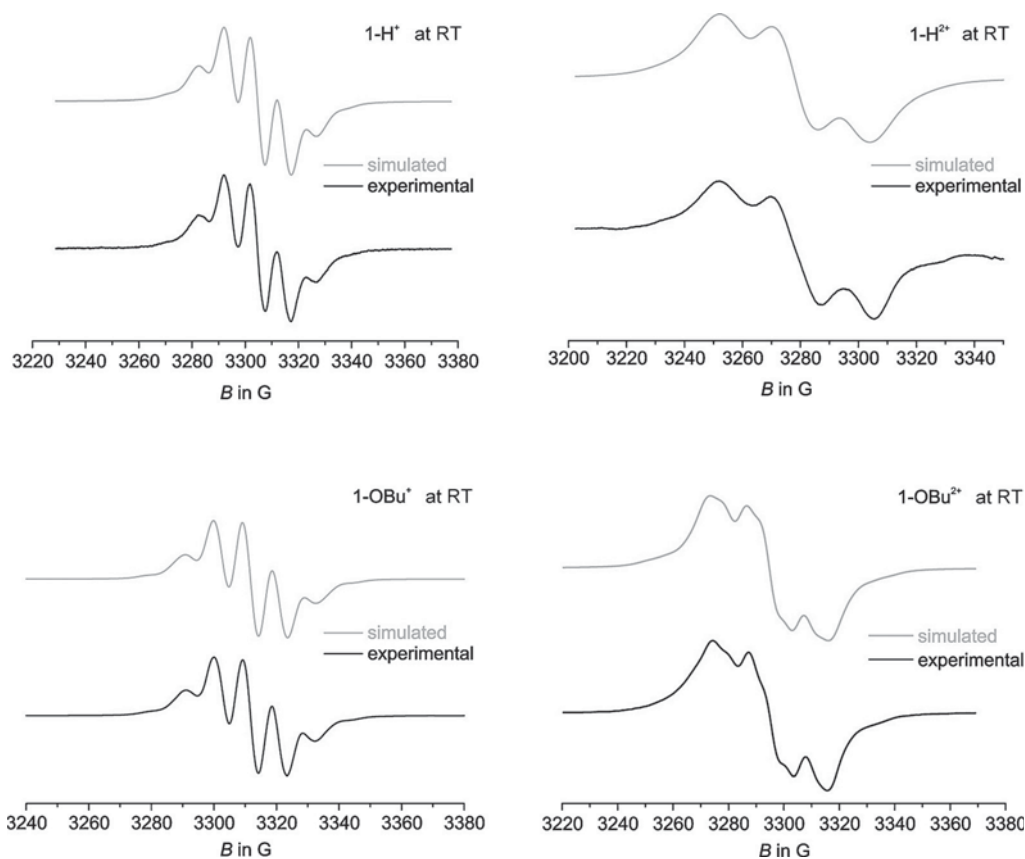


**Figure 8.** Simulated (top curve) and experimental (bottom curve) EPR spectra of  $1\text{ H}^+$  (top left), of  $1\text{ H}^{2+}$  (top right), of  $1\text{ OBU}^+$  (bottom left), and of  $1\text{ OBU}^{2+}$  (bottom right) in  $\text{CH}_2\text{Cl}_2$  solution at RT.

chibabin's hydrocarbons<sup>[29]</sup> (for recent reviews on that topic see reference [30]).

This prompted us to also study chemically prepared dications  $1\text{-H}^{2+}$  (oxidation with 1,1'-diacetylferrocenium hexafluoroantimonate) and  $1\text{-OBu}^{2+}$  (oxidation with acetylferrocenium hexafluoroantimonate). The dications gave persistent, deep blue solutions from which resolved EPR signals that are substantially different from those of the radical cations were recorded, as shown in Figure 8. The spectra were successfully simulated by assuming hfs interactions with two identical  $^{31}\text{P}$  nuclei, one  $^{99/101}\text{Ru}$  nucleus and two spin  $1/2$  nuclei with identical or slightly different hfs constants, which most probably are due to the vinylic or the *ortho*-phenylene hydrogen atoms. Most revealingly, the  $A(^{31}\text{P})$  and the  $A(^{99/101}\text{Ru})$  hfs constants are approximately twice those of the radical cations  $1\text{-H}^+$  and  $1\text{-OBu}^+$ , showing that the spin densities at the spin-bearing centers have accordingly increased on the introduction of a second unpaired spin. This may now also allow for the observation of resolved hfs to hydrogen nuclei, which were blurred by additional smaller couplings or the general line broadening in the radical cations. We also note that the hfs constants to  $^{31}\text{P}$  and  $^{99/101}\text{Ru}$  in  $1\text{-OBu}^+$  and  $1\text{-OBu}^{2+}$  are consistently smaller than those in  $1\text{-H}^+$  or  $1\text{-H}^{2+}$  while those to the hydrogen nuclei are larger, consistent with a higher bridge contribution to the relevant MOs for electron-rich  $1\text{-OBu}^{n+}$ . Again, the EPR signal persisted in frozen  $\text{CH}_2\text{Cl}_2$  solution at 103 K. On further cooling to 4 K the signal of  $1\text{-OBu}^{2+}$  even intensified, thus ruling out an open-shell singlet diradical ground-state (Figure 9). The magnetic susceptibility  $\chi$  calculated from double integration of  $T$ -dependent EPR spectra follows Curie's law  $\chi = C/T$ . The close adherence to the simple Curie's law indicates that the exchange coupling must be small. In spite of the high signal intensity we failed to observe the expected half-field signal for the  $\Delta m_s \pm 2$  transition, most probably because of the rather large spatial separation between the spin-bearing sites.<sup>[30a,31]</sup> In this context we note that, contrary to  $1\text{-H}^+$  and the singlet state of  $1\text{-H}^{2+}$ , the calculated spin density of the triplet state of  $1\text{-H}^{2+}$  concentrates on the ruthenium and the vinylic  $\beta$ -carbon atoms (see the following section). Tetra-cation  $3\text{-H}^{4+}$  may thus feature two paramagnetic  $\{[\text{Ru}] \text{CH}=\text{CH} \text{C}_6\text{H}_4 \text{CH}=\text{CH} [\text{Ru}]\}^{2+}$  units. Further studies will be directed at exploring that issue and that of magnetic interactions between the individual sides.

### Quantum chemistry

Earlier quantum chemical studies on  $1\text{-H}^{\text{Me} 2+}$ , a slightly truncated model complex of 1,4-divinylphenylene-bridged  $1\text{-H}$  bearing  $\text{PMe}_3$  instead of  $\text{P}i\text{Pr}_3$  ligands, had indicated that the antiferromagnetically coupled singlet state is energetically well above the ferromagnetically coupled triplet state.<sup>[11b]</sup> As our present EPR results disagree with these calculations we also studied the full model complex to find out whether this discrepancy is due to that simplification. Structure optimization<sup>[32]</sup> in 1,2- $\text{C}_2\text{H}_4\text{Cl}_2$  solvent accounted for within the framework of the CPCM<sup>[33]</sup> model resulted in a highly symmetrical and fully co-planar structure with a clear quinoidal distortion of the di-

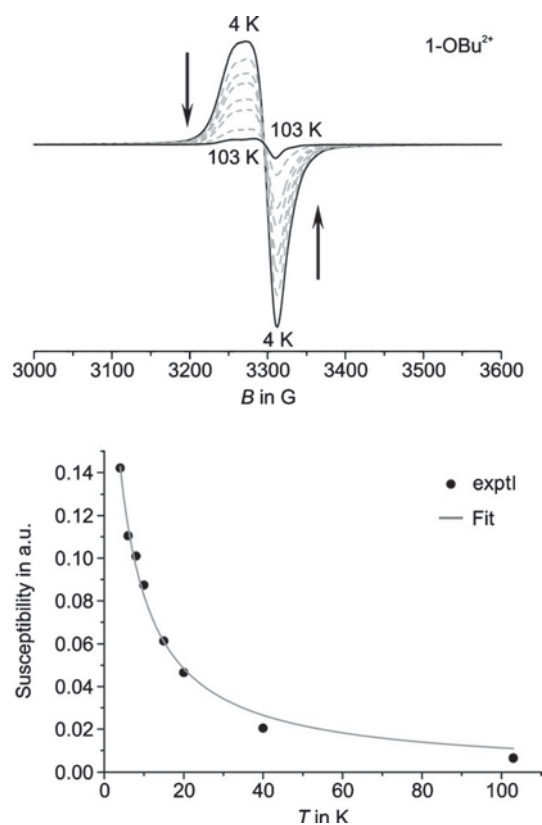


**Figure 9.** Top:  $T$  dependent EPR spectra of  $1\text{-OBu}^{2+}$  in  $\text{CH}_2\text{Cl}_2$  in the range from 4 to 103 K; bottom:  $T$  dependence of the magnetic susceptibility  $\chi$  (dots) and curve fit to Curie's law. The slight deviation for data points above 20 K was likewise observed for samples of the purely organic  $S = 1/2 \text{N}(\text{C}_6\text{H}_5\text{Br})_3^+$  radical cation. a. u. = arbitrary units.

vinylphenylene linker. Thus, on twofold oxidation, two opposing bonds of the central phenylene ring are computed to contract from 1.387 to 1.356 Å while the other four elongate from 1.406 and 1.407 Å to 1.422 and 1.423 Å, respectively. This translates into a quinoidal distortion parameter  $q$  of 95, which corresponds to an almost ideal quinoid structure.<sup>[34]</sup> Such structural alteration is well-known to promote or indicate closed-shell electronic ground states ( $S=0$ ) for 1,4-phenylene-bridged diradicals.<sup>[29a]</sup> Likewise, there is a shortening of the exocyclic C(phenyl) C(vinyl) and the Ru C(vinyl) bonds of 0.074 and 0.112 Å while the former C=C double bond elongates from 1.348 to 1.413 Å. More details can be retrieved from Table S2 in the Supporting Information. The triplet state is found 46.1  $\text{kJ mol}^{-1}$  above the singlet ground state and is computed to feature much smaller structural alterations within the conjugated bridging ligand when compared to the neutral and a much smaller quinoidal distortion ( $q=31$ ). Our attempts to calculate the open-shell singlet state produced the same general electronic structure of the closed-shell singlet state (only with spin orbitals instead of molecular orbitals) with essentially the same energy as the singlet ground state. Even the full computational model therefore does not reproduce the experimentally observed paramagnetism of complex  $1\text{-H}^{2+}$ .

As all our efforts to produce single crystals of any of the macrocyclic tetra-ruthenium compounds failed and in lieu of an

experimental crystal structure we performed detailed DFT calculations in order to arrive at an educated guess of their ground-state structures and to explore the conformational space. These calculations (PBE and PBE0)<sup>[32a-d,g,h]</sup> with the 1,2-C<sub>2</sub>H<sub>4</sub>Cl<sub>2</sub> or CHCl<sub>3</sub> solvent, accounted for by the polarizable conductor (CPCM)<sup>[33]</sup> or the COSMO-RS model,<sup>[35]</sup> were performed on the slightly truncated model complex **5-H**<sup>Me</sup> with PMe<sub>3</sub> instead of P*i*Pr<sub>3</sub> ligands. For model compound **5-H**<sup>Me</sup> the four low-energy structures shown in Figure 10 were identified. They differ in the orientations of the alkenyl ruthenium moieties with respect to the inner cavity of the metallamacrocycle. In the most stable conformer all metal-bonded vinyl groups point outward the inner cavity. This creates the most regular cavity with nonbonding H...H distances of 11.5 Å between the central CH units of the dicarboxylate linkers and of 7.5 Å between the hydrogen atoms of the bridging phenylene moieties. Two possible conformers, where two of the metal-bonded vinyl groups are oriented inward and the other two outward the cavity, are nearly isoenergetic and computed to be only 10 (PBE0) to 12 kJ mol<sup>-1</sup> (PBE) higher in energy than the most stable one. These two conformers differ with respect to whether the groups pointing inside the cage are part of the same 1,4-divinylphenylene side (conformer 2) or whether they belong to different ones to give a centrosymmetric structure (conformer 3). Conformer 4 has all Ru-CH moieties directed inward the cavity and is further 10 (PBE0) to 12 kJ mol<sup>-1</sup> (PBE) up in energy. This conformer possesses a rather prolate cavity. The DFT/pbe1pbe/TZVP/COSMO-RS(CHCl<sub>3</sub>) level of theory gave qualitatively similar data; energy differences to the most favorable conformer were, however higher (16.1 and 18.9 kJ mol<sup>-1</sup> for conformers 2 and 3 and 39.2 kJ mol<sup>-1</sup> for conformer 4 (Table S9 in the Supporting Information).

Structure parameters for the individual diruthenium divinylphenylene subunits taken from the optimized structures at the DFT/pbe1pbe/6-31G\*/PCM(1,2-C<sub>2</sub>H<sub>4</sub>Cl<sub>2</sub>) and the DFT/pbe1pbe/TZVP/COSMO-RS(CHCl<sub>3</sub>) levels of theory match well with those of other simple diruthenium 1,4-divinylphenylene complexes and do not exhibit any particular signs of strain (Table S9 in the Supporting Information).<sup>[11h,14f]</sup> Our calculated results further suggest that nearly all of the tetraruthenium macrocycles in solution (>98%) will be present as the minimum conformer.

Only this conformer was therefore considered for the various oxidized states. Interconversion between these structures will still occur by concerted rotations around two Ru-CH bonds. All stable conformers, however, have the divinylphenylene bridges in a lateral, side-by-side arrangement which shuts down  $\pi$ - $\pi$  interactions through space. Indeed, molecular orbitals with major contributions from the divinylphenylene bridges come as nearly degenerate pairs of MOs representing in- and out-of-phase combinations with energy splittings in the range of 0.07 to 0.09 eV (6.7 to 8.7 kJ mol<sup>-1</sup>). A representative example of the such MOs along with the MO scheme of **5-H**<sup>Me</sup> in the region of the frontier MOs is provided in Figure 11.

Our calculations thereby also rationalize the lack of electronic coupling through space as manifested by the experimentally observed charge and spin localization on just one diruthenium 1,4-divinylphenylene entity in the radical cations and the trications, where the two sites differ in their valence states. For both states structure optimizations gave two structurally different conjugated sides the structure parameters of which are basically identical to that of the neutral and the dication or the dication and tetracation, respectively (see Tables S10 and S11 in the Supporting Information). Spin and charge localization on just one diruthenium 1,4-divinylphenylene entity of complex **5-H**<sup>Me+</sup> also follow from the calculated  $\alpha$ -HOMO and the unpaired spin densities as shown in Figure 12 and the calculated Mulliken charges and spin densities in Tables S12–15 in the Supporting Information. This makes **5-H**<sup>+</sup> a mixed-valent system of Class I. The near invariance of the pyridyl fragment of the pyridine-3,5-dicarboxylate linkers to stepwise oxidation of macrocycle **5-H** is another token of its decoupling from the redox system and its insulating behavior.

Our computational results place the triplet state of dication **5-H**<sup>Me2+</sup> 61.5 kJ mol<sup>-1</sup> below the singlet state. As expected, charge and spin densities are evenly distributed over both diruthenium divinylphenylene sides. Graphical representations of the calculated spin orbitals and the MO scheme in the frontier orbital region and of the total spin densities are available in the Supporting Information (Figures S85–S88). For **5-H**<sup>Me3+</sup> the extra charge and spin are again confined to just one divinylphenylene diruthenium side such that the individual {Ru}-CH=C<sub>6</sub>H<sub>4</sub>-CH=CH-{Ru} entities differ in their intrinsic valence

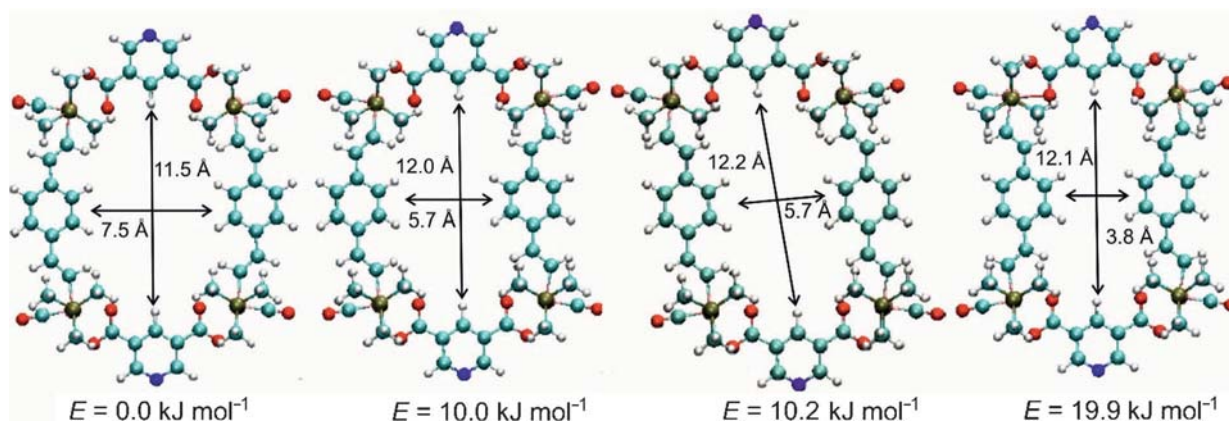
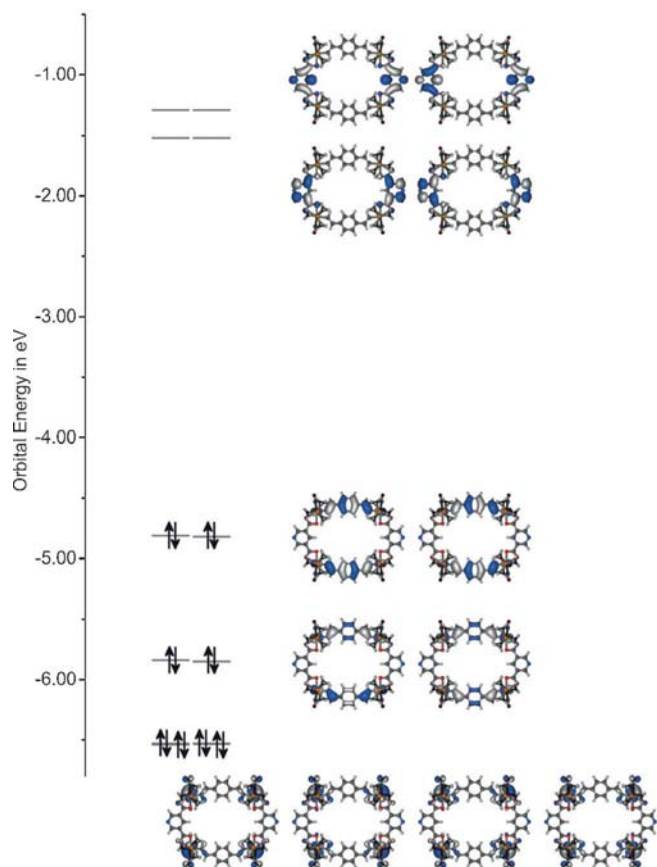
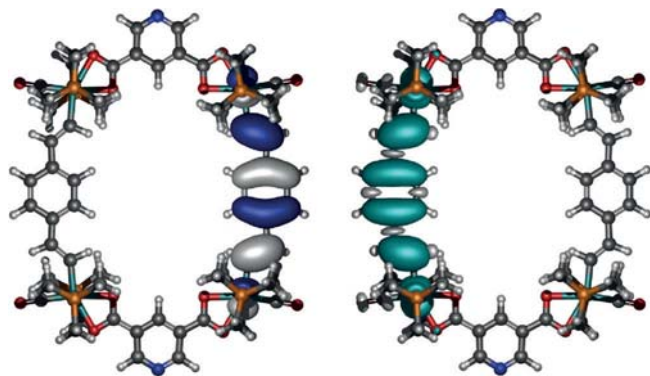


Figure 10. The four most stable conformers of the tetraruthenium model macrocycle **5-H**<sup>Me</sup>.



**Figure 11.** Partial MO scheme and graphical representations of frontier MOs of macrocycle  $5 \text{H}^{\text{Me}}$ .



**Figure 12.** The  $\alpha$  HOMO (left) and calculated spin densities (right) of  $5 \text{H}^{\text{Me}+}$ .

states, suggesting again Class I behavior with respect to ground-state electron delocalization *between* these units (Figures S86 and S87 in the Supporting Information).

According to our calculations, the quintet state of  $5\text{-H}^{\text{Me}4+}$  is  $488 \text{ kJ mol}^{-1}$  above the singlet state. It features two ferromagnetically coupled spins on every diruthenium 1,4-divinylphenylene side plus a ferromagnetic coupling between the individual divinylphenylene units. The majority of the spin density resides at the ruthenium and the vinylic  $\beta$ -carbon atoms along with smaller contributions of the phenylene bridges. Notably, no

spin density at all is found on the dicarboxylate linkers (Tables S14 and S15 and Figure S86 in the Supporting Information).

It is interesting that the spin densities do not match with the charge loss as expressed by changes in the Mulliken charges. This is particularly evident for  $5\text{-H}^{\text{Me}4+}$  in its quintet state. Thus, the majority of the charge loss is suffered by the *i*Pr substituents at the  $\text{P}i\text{Pr}_3$  co-ligands ( $1.20$  or  $1.60 \text{ e}^-$ , respectively), the divinylphenylene bridges ( $1.37$  or  $1.38 \text{ e}^-$ , respectively) and by the CO ligands ( $0.34$  or  $0.52 \text{ e}^-$ , respectively), while the total charge loss from the four ruthenium atoms amounts to  $0.87$  or only  $0.10$  electrons, depending on whether the DFT/pbe1pbe/6-31G\*/PCM(1,2- $\text{C}_2\text{H}_4\text{Cl}_2$ ) or the DFT/pbe1pbe/TZVP/COSMO-RS( $\text{CHCl}_3$ ) functional are used (Tables S12 and S13 in the Supporting Information). The same, albeit in an attenuated fashion, also holds for the triplet state of  $5\text{-H}^{\text{Me}2+}$  where the charge loss from the two ruthenium atoms sums up to  $0.4$  ( $0.04$ ) electrons ( $20$  or  $2\%$ ), while they carry  $31\%$  ( $34\%$ ) of the total spin density. The above results provide an interesting clue as to the particular ability of the  $\text{Ru}(\text{CO})\text{L}(\text{P}i\text{Pr}_3)_2$  ( $\text{L} = \text{Cl}^-$  or  $\kappa^2\text{-O,O'-RCOO}^-$ ) fragment to stabilize even higher oxidized forms of alkenyl ruthenium complexes and also indicate that charge and spin density distributions may well differ from each other.<sup>[36]</sup>

## Summary and Conclusions

We have successfully prepared four tetraruthenium metallacycles featuring two fully conjugated 1,4-divinylphenylene-bridged diruthenium entities  $\{\text{Ru}(\text{CO})\text{Cl}(\text{P}i\text{Pr}_3)_2\}_2(\mu\text{-}1,4\text{-CH=CH-C}_6\text{H}_2\text{R}_2\text{-CH=CH})$  ( $\text{R} = \text{H}$ : **1-H**;  $\text{R} = \text{O}i\text{Bu}$ : **1-OBu**) and two insulating benzene-1,3- (or 3,5-)dicarboxylate building blocks in moderate yields and have characterized them as such by multinuclear NMR and high resolution ESI MS spectroscopies. In some cases mixtures of tetra- and even larger hexaruthenium macrocycles featuring three pairs of divinylphenylene and dicarboxylate linkers are formed, which could, however, not be separated. The metallamacrocyclic compounds inherit the rich redox behavior of their 1,4-divinylphenylene-bridged diruthenium parents and are oxidized in four separate one-electron steps that come as pairs of two closely spaced one-electron waves, corresponding to the nearly coincident first and second oxidations of each conjugated side. Some small redox splitting between the  $0/+$  and  $+/2+$  and the  $2+/3+$  and the  $3+/4+$  waves can be resolved in some cases in the very weakly ion pairing  $\text{NBu}_4^+\text{B}\{\text{C}_6\text{H}_3(\text{CF}_3)_2\text{-}3,5\}_4^-$  electrolyte. Individual redox potentials respond to the electronic properties of the 1,4-divinylphenylene bridges and to those of the dicarboxylate linkers. Thus, introduction of the electron-donating butoxy substituents at the conjugated divinylphenylene sides decreases all half-wave potentials by about  $100 \text{ mV}$  (c.f. **5-H** versus **5-OBu**). Smaller shifts of about  $70 \text{ mV}$  are observed on replacing the amino substituent at the 5-position of the benzene-1,3-dicarboxylate linker in **3-H** by the cyano group (**4-H**) or by replacing the aniline core by pyridine (**5-H**).

In depth IR and UV/Vis/NIR spectroelectrochemical investigations on all macrocyclic complexes show that the splitting ob-

served for the 0/+ and +/2+ and the 2+/3+ and 3+/4+ waves is entirely due to electrostatic effects. Thus, none of the IR and UV/Vis/NIR spectra recorded when slowly scanning through the composite 0/+ and +/2+ waves or the 2+/3+ and 3+/4+ waves shows any additional absorption band(s) that could be ascribed to electron transfer between the reduced and the oxidized 1,4-divinylphenylene diruthenium sides of every macrocycle (i.e., "intracage" electron transfer), albeit the radical cations and trications constitute the dominant species in solution after release of one or three electrons per macrocycle. Our studies also show that the macrocycles fully retain the known electrochromic behavior of the 1,4-divinylphenylene building blocks with the obvious consequence that molar extinction coefficients are doubled owing to the presence of two such chromophores in the same system.

The mutual insulation of the divinylphenylene linkers has the interesting consequence of rendering their dioxidized, dicationic forms paramagnetic. Thus, all dications of these macrocycles give a strong, isotropic EPR signal in fluid and in frozen solution at  $g \approx 2.040$  that does not exhibit a half-field signal for the  $\Delta m_s \pm 2$  transition. This points to a paramagnetic ground state with two non-interacting spins. Even more surprisingly, the tetracation of macrocycle **3-H** (**3-H<sup>4+</sup>**), where all 1,4-divinylphenylene sides are oxidized by two electrons, also shows an EPR signal in fluid and in frozen solution, albeit of only weak intensity. This prompted us to also study the dications of the 1,4-divinylphenylene diruthenium precursors by EPR spectroscopy. To our surprise, and contrary to our quantum chemical calculations, both showed an intense EPR signal with resolved hyperfine interactions to the  $^{31}\text{P}$  nuclei of the two  $\text{P}i\text{Pr}_3$  co-ligands at the ruthenium atom, the  $^{99/101}\text{Ru}$  nucleus itself and two vinyl or aryl protons. The former are twice as large as those in the radical cations, where one unpaired spin is completely delocalized over the entire  $\{\text{Ru}\} \text{CH}=\text{CH} \text{C}_6\text{H}_4 \text{CH}=\text{CH} \{\text{Ru}\}$  backbone. The magnetic ground state of that dication was further explored by low-temperature EPR spectroscopy down to 4 K. On cooling, the signal intensity increased in accord with simple Curie's law. Our failure to observe any magnetic coupling and the absence of a half-field signal for the  $\Delta m_s \pm 2$  transition points to two non-interacting (or very weakly interacting) spins and an open-shell ground state. Such highly unusual behavior, while not completely unknown, has rather little literature precedence.<sup>[28]</sup> On the other hand, the increase of the magnetization at low  $T$  and the adherence to Curie's law clearly argue against an open-shell singlet ground state as it has been recently documented for closely related 1,4-phenylene or 4,4'-biphenyl-bridged bis(diarylammonium) dications.<sup>[29]</sup> The open-shell singlet ground states of the latter systems are supported by the ability of the peripheral redox sites to delocalize the unpaired spin(s) and by the

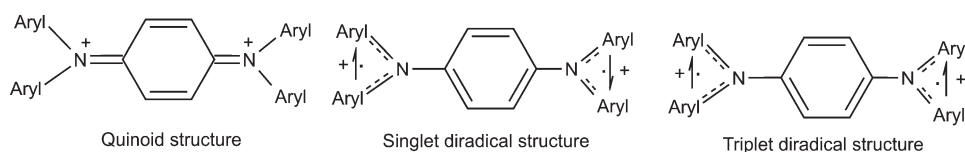
reluctance of the bridging arylene moieties to sacrifice aromatic stabilization in favor of a quinoidal structure (Scheme 2). The same overall mechanism could be operative here owing to the likewise high ability of the  $\text{Ru}(\text{CO})\text{L}(\text{P}i\text{Pr}_3)_2$  ( $\{\text{Ru}\}$ ) appendices to accommodate unpaired spin density.

The latter is clearly borne out by our quantum chemical calculations. Thus, the majority of the spin density in open-shell states of the 1,4-divinylphenylene building blocks as well as that of oxidized model macrocycle **5-H<sup>Me n+</sup>** resides at the  $\{\text{Ru}\}$  moieties with only smaller contributions from the nominal bridge. In contrast, oxidation induces only minor charge loss from the metal atoms themselves. The majority of the charge is extracted from the conjugated 1,4-divinylphenylene bridges and, notably, the  $\text{P}i\text{Pr}_3$  co-ligands. This finally provides a clue as to the superior ability of the  $\text{P}i\text{Pr}_3$  ligands to stabilize the oxidized forms of alkenyl complexes of the  $\text{Ru}(\text{CO})\text{Cl}(\text{P}i\text{Pr}_3)_2$  or the  $\text{Ru}(\text{CO})(\text{P}i\text{Pr}_3)_2(\kappa\text{O},\text{O}'\text{-OOCR})$  tags. Nonetheless, further studies are warranted in order to fully understand the magnetic properties of highly oxidized arylene-bridged alkenyl ruthenium complexes of higher nuclearity and the macrocyclic structures formed from such building blocks. We also have to concede that our quantum chemical calculations failed to reproduce the experimentally observed paramagnetic ground state for the full model **1-H<sup>2+</sup>** by placing the triplet and open-shell singlet states well above the singlet ground state. On the other hand, they correctly predict an open-shell triplet ground state for the dications of the macrocycles.

As all our attempts at growing crystals of any of these macrocyclic tetra-ruthenium complexes failed, we resorted to quantum chemical calculations to obtain a glimpse of their likely structures and to explore their conformational space. Four reasonably low-lying conformers were localized on the potential hypersurface that differ with respect to the orientation of the vinyl groups (outward or inward) with respect to the inner cavity of the macrocycles. All of them have the 1,4-divinylphenylene and dicarboxylate entities in rather relaxed geometries and do not exhibit any particular signs of strain. All of them agree, however, in positioning the divinylphenylene linkers in a co-lateral side-by-side arrangement as opposed to a stacked face-to-face orientation. This, together with the insulating behavior of the dicarboxylate linkers, shuts down intramolecular charge transfer between the differently charged divinylphenylene diruthenium sides in the mixed-valent 1+ and 3+ charge states in accordance with our experimental observations.

## Experimental Section

Detailed information can be found in the Supporting Information. The document includes experimental procedures and details to the quantum chemical calculations and the synthesis and characteriza-



**Scheme 2.** Possible electronic structures of phenylene bridged bis(diarylammonium) dications.

tion of all compounds (NMR, HR ESI-MS); details of the X-ray crystallographic structure determination of **1-OBu** and **1-OBu-2CHCl<sub>3</sub>**; graphical accounts of the NMR and ESI MS spectra; representative cyclic and square wave voltammograms of all compounds; Figures showing the outcome of IR and UV/Vis/NIR spectroelectrochemical studies on all compounds; Figures showing the EPR spectra; Figure showing the MO schemes in the frontier MO region and, if applicable, the spin densities of model macrocycle **5-H<sup>Me</sup>** in different charge and spin states; Tables providing the calculated structure parameters, MO compositions according to Mulliken analysis and the charge and spin densities for various fragments for the full model **1-H** and macrocycle **5-H<sup>Me</sup>** in their various charge and spin states.

CCDC 1469982 and 1469983 contain the supplementary crystallographic data for this paper. These data are provided free of charge by The Cambridge Crystallographic Data Centre.

## Acknowledgements

We gratefully acknowledge financial support by the German Research Foundation (DFG) through Collaborative Research Center (SFB) 767, and the Carl-Zeiss Foundation. This work was supported by the bwHPC program through the computational resources of the bwUniCluster and the JUSTUS HPC facility. We also thank Steffen Oßwald for his aid with the graphical material.

**Keywords:** (spectro)electrochemistry · density functional calculations · electrochromism · metallamacrocyclic · paramagnetism

- [1] a) M. Fujita, M. Tominaga, A. Hori, B. Therrien, *Acc. Chem. Res.* **2005**, *38*, 369–378; b) C. G. Oliveri, P. A. Ulmann, M. J. Wiester, C. A. Mirkin, *Acc. Chem. Res.* **2008**, *41*, 1618–1629; c) Y. F. Han, W. G. Jia, W. B. Yu, G. X. Jin, *Chem. Soc. Rev.* **2009**, *38*, 3419–3434; d) R. Chakrabarty, P. S. Mukherjee, P. J. Stang, *Chem. Rev.* **2011**, *111*, 6810–6918; e) B. Lippert, P. J. Sanz Miguel, *Chem. Soc. Rev.* **2011**, *40*, 4475–4487; f) M. M. J. Smulders, I. A. Riddell, C. Browne, J. R. Nitschke, *Chem. Soc. Rev.* **2013**, *42*, 1728–1754; g) M. Han, D. M. Engelhard, G. H. Clever, *Chem. Soc. Rev.* **2014**, *43*, 1848–1860.
- [2] a) M. D. Ward, P. R. Raithby, *Chem. Soc. Rev.* **2013**, *42*, 1619–1636; b) A. Mishra, S. C. Kang, K. W. Chi, *Eur. J. Inorg. Chem.* **2013**, 5222–5232; c) A. Schmidt, A. Casini, F. E. Kühn, *Coord. Chem. Rev.* **2014**, *275*, 19–36; d) R. Custelcean, *Chem. Soc. Rev.* **2014**, *43*, 1813–1824.
- [3] a) S. Shanmugaraju, A. K. Bar, K. W. Chi, P. S. Mukherjee, *Organometallics* **2010**, *29*, 2971–2980; b) S. Shanmugaraju, S. A. Joshi, P. S. Mukherjee, *Inorg. Chem.* **2011**, *50*, 11736–11745; c) L. Xu, Y. X. Wang, H. B. Yang, *Dalton Trans.* **2015**, *44*, 867–890.
- [4] a) S. Tashiro, M. Tominaga, M. Kawano, B. Therrien, T. Ozeki, M. Fujita, *J. Am. Chem. Soc.* **2005**, *127*, 4546–4547; b) N. P. E. Barry, O. Zava, P. J. Dyson, B. Therrien, *J. Organomet. Chem.* **2012**, *705*, 1–6; c) J. E. M. Lewis, E. L. Gavey, S. A. Cameron, J. D. Crowley, *Chem. Sci.* **2012**, *3*, 778–784.
- [5] a) B. Therrien, *Eur. J. Inorg. Chem.* **2009**, 2445–2453; b) J. Mattsson, P. Govindaswamy, A. K. Renfrew, P. J. Dyson, P. Štěpnička, G. Süß Fink, B. Therrien, *Organometallics* **2009**, *28*, 4350–4357; c) N. P. E. Barry, F. Edafe, B. Therrien, *Dalton Trans.* **2011**, *40*, 7172–7180; d) T. R. Cook, V. Vajpayee, M. H. Lee, P. J. Stang, K. W. Chi, *Acc. Chem. Res.* **2013**, *46*, 2464–2474; e) A. Garci, A. A. Dobrov, T. Riedel, E. Orhan, P. J. Dyson, V. B. Arion, B. Therrien, *Organometallics* **2014**, *33*, 3813–3822.
- [6] a) Y. Nishioka, T. Yamaguchi, M. Yoshizawa, M. Fujita, *J. Am. Chem. Soc.* **2007**, *129*, 7000–7001; b) S. Horiuchi, T. Murase, M. Fujita, *Chem. Asian J.* **2011**, *6*, 1839–1847; c) W. Z. Zhang, Y. F. Han, Y. J. Lin, G. X. Jin, *Organometallics* **2010**, *29*, 2842–2849.
- [7] a) P. H. Dinolfo, M. E. Williams, C. L. Stern, J. T. Hupp, *J. Am. Chem. Soc.* **2004**, *126*, 12989–13001; b) P. H. Dinolfo, J. T. Hupp, *J. Am. Chem. Soc.* **2004**, *126*, 16814–16819; c) P. H. Dinolfo, S. J. Lee, V. Coropceanu, J. L. Brédas, J. T. Hupp, *Inorg. Chem.* **2005**, *44*, 5789–5797; d) P. H. Dinolfo, V. Coropceanu, J. L. Brédas, J. T. Hupp, *J. Am. Chem. Soc.* **2006**, *128*, 12592–12593.
- [8] M. B. Robin, P. Day, *Adv. Inorg. Chem. Radiochem.* **1967**, *10*, 247–422.
- [9] a) H. Hartmann, S. Berger, R. Winter, J. Fiedler, W. Kaim, *Inorg. Chem.* **2000**, *39*, 4977–4980; b) W. Kaim, B. Schwederski, A. Dogan, J. Fiedler, C. J. Kuehl, P. J. Stang, *Inorg. Chem.* **2002**, *41*, 4025–4028; c) N. Das, A. M. Arif, P. J. Stang, M. Sieger, B. Sarkar, W. Kaim, J. Fiedler, *Inorg. Chem.* **2005**, *44*, 5798–5804; d) V. Vajpayee, S. Bivaud, S. Goeb, V. Croué, M. Allain, B. V. Popp, A. Garci, B. Therrien, M. Sallé, *Organometallics* **2014**, *33*, 1651–1658; e) M. Yuan, F. Weisser, B. Sarkar, A. Garci, P. Braunstein, L. Routaboul, B. Therrien, *Organometallics* **2014**, *33*, 5043–5045.
- [10] a) M. O’Keeffe, O. M. Yaghi, *Chem. Rev.* **2012**, *112*, 675–702; b) T. R. Cook, Y. R. Zheng, P. J. Stang, *Chem. Rev.* **2013**, *113*, 734–777; c) W. Lu, Z. Wei, Z. Y. Gu, T. F. Liu, J. Park, J. Tian, M. Zhang, Q. Zhang, T. Gentle III, M. Bosch, H. C. Zhou, *Chem. Soc. Rev.* **2014**, *43*, 5561–5593.
- [11] a) J. Maurer, R. F. Winter, B. Sarkar, J. Fiedler, S. Zálíš, *Chem. Commun.* **2004**, 1900–1901; b) J. Maurer, B. Sarkar, B. Schwederski, W. Kaim, R. F. Winter, S. Zálíš, *Organometallics* **2006**, *25*, 3701–3712; c) J. Maurer, B. Sarkar, W. Kaim, R. F. Winter, S. Zálíš, *Chem. Eur. J.* **2007**, *13*, 10257–10272; d) F. Pevny, E. Di Piazza, L. Norel, M. Drescher, R. F. Winter, S. Rigaut, *Organometallics* **2010**, *29*, 5912–5918; e) P. Mücke, M. Linseis, S. Zálíš, R. F. Winter, *Inorg. Chim. Acta* **2011**, *374*, 36–50; f) M. Linseis, S. Zálíš, M. Zabel, R. F. Winter, *J. Am. Chem. Soc.* **2012**, *134*, 16671–16692; g) R. F. Winter, *Organometallics* **2014**, *33*, 4517–4536; h) E. Wuttke, Y. M. Hervault, W. Polit, M. Linseis, P. Erler, S. Rigaut, R. F. Winter, *Organometallics* **2014**, *33*, 4672–4686; i) J. L. Xia, W. Y. Man, X. Zhu, C. Zhang, G. J. Jin, P. A. Schauer, M. A. Fox, J. Yin, G. A. Yu, P. J. Low, S. H. Liu, *Organometallics* **2012**, *31*, 5321–5333; j) Y. Lin, J. Yuan, M. Hu, J. Yin, S. Jin, S. H. Liu, *Organometallics* **2009**, *28*, 6402–6409; k) X. H. Wu, S. Jin, J. H. Liang, Z. Yong, G. a. Yu, S. H. Liu, *Organometallics* **2009**, *28*, 2450–2459; l) F. Li, J. Cheng, X. Chai, S. Jin, X. Wu, G. A. Yu, S. H. Liu, G. Z. Chen, *Organometallics* **2011**, *30*, 1830–1837; m) W. Y. Man, J. L. Xia, N. J. Brown, J. D. Farmer, D. S. Yufit, J. A. K. Howard, S. H. Liu, P. J. Low, *Organometallics* **2011**, *30*, 1852–1858; n) J. Zhang, Y. Ou, M. Xu, C. Sun, J. Yin, G. A. Yu, S. H. Liu, *Eur. J. Inorg. Chem.* **2014**, 2941–2951.
- [12] a) M. Linseis, R. F. Winter, B. Sarkar, W. Kaim, S. Zálíš, *Organometallics* **2008**, *27*, 3321–3324; b) W. Polit, T. Exner, E. Wuttke, R. F. Winter, *Biol. Inorg. Chem. Rev.* **2012**, *8*, 85–105; c) U. Pfaff, A. Hildebrandt, M. Korb, S. Oßwald, M. Linseis, K. Schreiter, S. Spange, R. F. Winter, H. Lang, *Chem. Eur. J.* **2016**, *22*, 783–801; d) E. Wuttke, D. Fink, P. Anders, A. L. M. Hoyt, W. Polit, M. Linseis, R. F. Winter, *J. Organomet. Chem.* **2016**; DOI: 10.1016/j.jorganchem.2016.02.031.
- [13] O. S. Abdel Rahman, J. Maurer, S. Zálíš, R. F. Winter, *Organometallics* **2015**, *34*, 3611–3628.
- [14] a) H. Loumrhari, J. Ros, M. R. Torres, A. Perales, *Polyhedron* **1990**, *9*, 907–911; b) M. R. Torres, A. Perales, H. Loumrhari, J. Ros, *J. Organomet. Chem.* **1990**, *385*, 379–386; c) M. E. Guaouzi, J. Ros, X. Solans, M. Font Bardía, *Inorg. Chim. Acta* **1995**, *231*, 181–186; d) L. Matas, I. Moldes, J. Soler, J. Ros, Á. Alvarez Larena, J. F. Piniella, *Organometallics* **1998**, *17*, 4551–4555; e) S. Jung, C. D. Brandt, J. Wolf, H. Werner, *Dalton Trans.* **2004**, 375–383; f) F. Pevny, R. F. Winter, B. Sarkar, S. Zálíš, *Dalton Trans.* **2010**, 39, 8000–8011; g) S. Naeem, A. Ribes, A. J. P. White, M. N. Haque, K. B. Holt, J. D. E. T. Wilton Ely, *Inorg. Chem.* **2013**, *52*, 4700–4713; h) Y. H. Lin, L. Duclaux, F. González de Rivera, A. L. Thompson, J. D. E. T. Wilton Ely, *Eur. J. Inorg. Chem.* **2014**, 2065–2072.
- [15] a) M. A. Esteruelas, H. Werner, *J. Organomet. Chem.* **1986**, *303*, 221–231; b) H. Werner, U. Meyer, K. Peters, H. G. von Schnering, *Chem. Ber.* **1989**, *122*, 2089–2107; c) M. R. Torres, A. Vegas, A. Santos, *J. Organomet. Chem.* **1986**, *309*, 169–177; d) A. F. Hill, in *Comprehensive Organometallic Chemistry II, Vol. 7* (Eds.: D. E. Shriver, M. I. Bruce), Pergamon, Oxford, **1995**, pp. 399–411; e) A. V. Marchenko, H. Gérard, O. Eisenstein, K. G. Caulton, *New J. Chem.* **2001**, *25*, 1382–1388; f) A. V. Marchenko, H. Gérard, O. Eisenstein, K. G. Caulton, *New J. Chem.* **2001**, *25*, 1244–1255; g) S. K. Seetharaman, M. C. Chung, U. Englisch, K. Ruhlandt Senge, M. B. Sponser, *Inorg. Chem.* **2007**, *46*, 561–567.

- [16] E. Wuttke, F. Pevny, Y. M. Hervault, L. Norel, M. Drescher, R. F. Winter, S. Rigaut, *Inorg. Chem.* **2012**, *51*, 1902–1915.
- [17] a) H. Werner, M. A. Esteruelas, H. Otto, *Organometallics* **1986**, *5*, 2295–2299; b) D. Huang, W. E. Streib, J. C. Bollinger, K. G. Caulton, R. F. Winter, T. Scheiring, *J. Am. Chem. Soc.* **1999**, *121*, 8087–8097; c) Y. Maruyama, K. Yamamura, T. Sagawa, H. Katayama, F. Ozawa, *Organometallics* **2000**, *19*, 1308–1318; d) S. Jung, K. Ilg, C. D. Brandt, J. Wolf, H. Werner, *Eur. J. Inorg. Chem.* **2004**, 469–480; e) J. Maurer, M. Linseis, B. Sarkar, B. Schwederski, M. Niemeyer, W. Kaim, S. Zálíš, C. Anson, M. Zabel, R. F. Winter, *J. Am. Chem. Soc.* **2008**, *130*, 259–268; f) P. Mücke, M. Zabel, R. Edge, D. Collison, S. Clément, S. Zálíš, R. F. Winter, *J. Organomet. Chem.* **2011**, *696*, 3186–3197; g) K. Kowalski, M. Linseis, R. F. Winter, M. Zabel, S. Zálíš, H. Kelm, H. J. Krüger, B. Sarkar, W. Kaim, *Organometallics* **2009**, *28*, 4196–4209; h) W. Polt, P. Mücke, E. Wuttke, T. Exner, R. F. Winter, *Organometallics* **2013**, *32*, 5461–5472.
- [18] a) M. D. Geraldo, M. I. Montenegro, L. Slevin, D. Pletcher, *J. Phys. Chem. B* **2001**, *105*, 3182–3186; b) N. A. Macías Ruvalcaba, D. H. Evans, *J. Phys. Chem. B* **2005**, *109*, 14642–14647; c) P. Hapiot, L. D. Kispert, V. Y. Konovalov, J. M. Savéant, *J. Am. Chem. Soc.* **2001**, *123*, 6669–6677; d) F. Barrière, N. Camire, W. E. Geiger, U. T. Mueller Westerhoff, R. Sanders, *J. Am. Chem. Soc.* **2002**, *124*, 7262–7263; e) F. Barrière, W. E. Geiger, *J. Am. Chem. Soc.* **2006**, *128*, 3980–3989; f) C. J. Adams, R. C. da Costa, R. Edge, D. H. Evans, M. F. Hood, *J. Org. Chem.* **2010**, *75*, 1168–1178.
- [19] S. Zálíš, R. F. Winter, W. Kaim, *Coord. Chem. Rev.* **2010**, *254*, 1383–1396.
- [20] a) P. Mücke, R. F. Winter, I. Novak, K. Kowalski, *J. Organomet. Chem.* **2012**, *717*, 14–22; b) P. Mücke, R. F. Winter, K. Kowalski, *J. Organomet. Chem.* **2013**, *735*, 10–14.
- [21] a) D. E. Richardson, H. Taube, *Coord. Chem. Rev.* **1984**, *60*, 107–129; b) S. Santi, A. Bisello, R. Cardena, A. Donoli, *Dalton Trans.* **2015**, *44*, 5234–5257.
- [22] M. Krejčík, M. Daněk, F. Hartl, *J. Electroanal. Chem.* **1991**, *317*, 179–187.
- [23] a) K. Costuas, O. Cador, F. Justaud, S. Le Stang, F. Paul, A. Monari, S. Evangelisti, L. Toupet, C. Lapinte, J. F. Halet, *Inorg. Chem.* **2011**, *50*, 12601–12622; b) E. C. Fitzgerald, A. Ladjarafi, N. J. Brown, D. Collison, K. Costuas, R. Edge, J. F. Halet, F. Justaud, P. J. Low, H. Meghezzi, T. Roisnel, M. W. Whiteley, C. Lapinte, *Organometallics* **2011**, *30*, 4180–4195; c) M. Parthey, J. B. G. Gluyas, M. A. Fox, P. J. Low, M. Kaupp, *Chem. Eur. J.* **2014**, *20*, 6895–6908.
- [24] a) N. Deibel, M. G. Sommer, S. Hohloch, J. Schwann, D. Schweinfurth, F. Ehret, B. Sarkar, *Organometallics* **2014**, *33*, 4756–4765; b) W. Kaim, *Coord. Chem. Rev.* **2011**, *255*, 2503–2513.
- [25] A. B. P. Lever, in *Comprehensive Organometallic Chemistry, Vol. 2*, Elsevier, Amsterdam, **2003**, pp. 435–438.
- [26] a) A. A. Ovchinnikov, *Theor. Chim. Acta* **1978**, *47*, 297–304; b) O. Kahn, *Molecular Magnets*, VCH, Weinheim, **1993**.
- [27] a) K. Yoshizawa, R. Hoffmann, *Chem. Eur. J.* **1995**, *1*, 403–413; b) J. Zhang, H. Zhang, L. Wang, R. Wang, L. Wang, *Sci. China Ser. B* **2000**, *43*, 524–530; c) M. Baumgarten, in *EPR of Free Radicals in Solids II* (Eds.: A. Lund, M. Shiotani), Springer, Heidelberg, **2012**, pp. 205–244.
- [28] a) K. Inoue, H. Iwamura, *Angew. Chem. Int. Ed. Engl.* **1995**, *34*, 927–928; *Angew. Chem.* **1995**, *107*, 973–975; b) K. Okada, T. Imakura, M. Oda, H. Murai, M. Baumgarten, *J. Am. Chem. Soc.* **1996**, *118*, 3047–3048; c) R. Chiarelli, S. Gambarelli, A. Rassat, *Mol. Cryst. Liq. Cryst.* **1997**, *305*, 455–478; d) Y. Hosokoshi, Y. Nakazawa, K. Inoue, K. Takizawa, H. Nakano, M. Takahashi, T. Goto, *Phys. Rev. B* **1999**, *60*, 12924–12932; e) H. Kumagai, Y. Hosokoshi, A. S. Markosyan, K. Inoue, *Polyhedron* **2001**, *20*, 1329–1333; f) G. Trinquier, J. P. Malrieu, *Chem. Eur. J.* **2015**, *21*, 814–828.
- [29] a) K. Fukuda, M. Nakano, *J. Phys. Chem. A* **2014**, *118*, 3463–3471; b) Y. Su, X. Wang, Y. Li, Y. Song, Y. Sui, X. Wang, *Angew. Chem. Int. Ed.* **2015**, *54*, 1634–1637; *Angew. Chem.* **2015**, *127*, 1654–1657; c) Z. Zeng, S. Lee, M. Son, K. Fukuda, P. M. Burrezo, X. Zhu, Q. Qi, R. W. Li, J. T. L. Navarrete, J. Ding, J. Casado, M. Nakano, D. Kim, J. Wu, *J. Am. Chem. Soc.* **2015**, *137*, 8572–8583.
- [30] a) M. Abe, *Chem. Rev.* **2013**, *113*, 7011–7088; b) Z. Sun, Z. Zeng, J. Wu, *Chem. Asian J.* **2013**, *8*, 2894–2904; c) Z. Sun, J. Wu, *J. Mater. Chem.* **2012**, *22*, 4151–4160; d) J. Casado, R. Ponce Ortiz, J. T. Lopez Navarrete, *Chem. Soc. Rev.* **2012**, *41*, 5672–5686.
- [31] a) T. Koide, K. Furukawa, H. Shinokubo, J. Y. Shin, K. S. Kim, D. Kim, A. Osuka, *J. Am. Chem. Soc.* **2010**, *132*, 7246–7247; b) Y. Li, W. K. Heng, B. S. Lee, N. Aratani, J. L. Zafra, N. Bao, R. Lee, Y. M. Sung, Z. Sun, K. W. Huang, R. D. Webster, J. T. López Navarrete, D. Kim, A. Osuka, J. Casado, J. Ding, J. Wu, *J. Am. Chem. Soc.* **2012**, *134*, 14913–14922.
- [32] a) Gaussian 09, Revision B.01, M. J. Frisch, G. Trucks, H. B. Schlegel, G. E. Scuseria, M. A. Robb, J. R. Cheeseman, G. Scalmani, V. Barone, B. Menonucci, G. A. Petersson, H. Nakatsuji, M. Caricato, X. Li, H. P. Hratchian, A. F. Izmaylov, J. Blonio, G. Zheng, J. L. Sonnenberg, M. Hada, M. Ehara, K. Toyota, R. Fukuda, J. Hasegawa, M. Ishida, T. Nakajima, Y. Honda, O. Kitao, H. Nakai, T. Vreven, J. A. Montgomery, Jr., J. E. Peralta, F. Ogliaro, M. Bearpark, J. J. Heyd, E. Brothers, K. N. Kudin, V. N. Staroverov, T. Keith, R. Kobayashi, J. Normand, K. Raghavachari, A. Rendell, J. C. Burant, S. S. Iyengar, J. Tomasi, M. Cossi, N. Rega, J. M. Millam, M. Klene, J. E. Knox, J. B. Cross, V. Bakken, C. Adamo, J. Jaramillo, R. Gomperts, R. E. Stratmann, O. Yazyev, A. J. Austin, R. Cammi, C. Pomelli, J. W. Ochterski, R. L. Martin, K. Morokuma, V. G. Zakrzewski, G. A. Voth, P. Salvador, J. J. Dannenberg, S. Dapprich, A. D. Daniels, Ö. Farkas, J. B. Foresman, J. V. Ortiz, J. Cioslowski, D. J. Fox, Gaussian Inc., Wallingford, CT, **2010**; b) TURBO MOLE V6.5, a development of University of Karlsruhe and Forschungszentrum Karlsruhe GmbH, 1989–2007, TURBOMOLE GmbH, since 2007; available from <http://www.turbomole.com>; c) M. Dolg, H. Stoll, H. Preuss, *J. Chem. Phys.* **1989**, *90*, 1730–1734; d) W. Küchle, M. Dolg, H. Stoll, H. Preuss, *J. Chem. Phys.* **1994**, *100*, 7535; e) D. Andrae, U. Haeusermann, M. Dolg, H. Stoll, H. Preuss, *Theor. Chim. Acta* **1990**, *77*, 123; f) P. H. Hariharan, J. A. Pople, *Theor. Chim. Acta* **1973**, *28*, 213–222; g) J. P. Perdew, K. Burke, M. Enzerhof, *Phys. Rev. Lett.* **1996**, *77*, 3865–3868; h) C. Adamo, V. Barone, *J. Chem. Phys.* **1999**, *110*, 6158–6170; i) A. Schäfer, H. Horn, R. Ahlrichs, *J. Chem. Phys.* **1992**, *97*, 2571–2577.
- [33] M. Cossi, N. Rega, G. Scalmani, V. Barone, *J. Comput. Chem.* **2003**, *24*, 669–681.
- [34] a) R. Rathore, S. V. Lindeman, A. S. Kumar, J. K. Kochi, *J. Am. Chem. Soc.* **1998**, *120*, 6931–6939; b) D. Sun, S. V. Lindeman, R. Rathore, J. K. Kochi, *J. Chem. Soc. Perkin Trans. 2* **2001**, 1585–1594.
- [35] F. Eckert, A. Klamt, *AIChE J.* **2002**, *48*, 369–385.
- [36] M. E. Stoll, S. R. Lovelace, W. E. Geiger, H. Schimanke, I. Hyla Kryspin, R. Gleiter, *J. Am. Chem. Soc.* **1999**, *121*, 9343–9351.